IOP Publishing Phys. Biol. 17 (2020) 036004 https://doi.org/10.1088/1478-3975/ab725c

Physical Biology

PAPER

A biomechanical model for the transendothelial migration of cancer cells

RECEIVED
24 October 2019

REVISED
29 January 2020

ACCEPTED FOR PUBLICATION
3 February 2020

PUBLISHED
19 March 2020

S M Amin Arefi[1], Daria Tsvirkun[2,3], Claude Verdier[2] and James J Feng[1,4,5]

[1] Department of Chemical and Biological Engineering, University of British Columbia, Vancouver, BC V6T 1Z3, Canada
[2] University Grenoble Alpes, CNRS, LIPhy, 38000 Grenoble, France
[3] Belozersky Institute of Physico-chemical Biology, Lomonosov Moscow State University, Moscow 119991, Russia
[4] Department of Mathematics, University of British Columbia, Vancouver, BC V6T 1Z2, Canada
[5] Author to whom any correspondence should be addressed.

E-mail: james.feng@ubc.ca

Keywords: transmigration, stress fibers, focal adhesion, invadopodia, metastasis, cell mechanics, atomic-force microscopy

Supplementary material for this article is available online

Abstract

We propose a biomechanical model for the extravasation of a tumor cell (TC) through the endothelium of a blood vessel. Based on prior *in vitro* observations, we assume that the TC extends a protrusion between adjacent endothelial cells (ECs) that adheres to the basement membrane via focal adhesions (FAs). As the protrusion grows in size and branches out, the actomyosin contraction along the stress fibers (SFs) inside the protrusion pulls the relatively rigid nucleus through the endothelial opening. We model the chemo-mechanics of the SFs and the FAs by following the kinetics of the active myosin motors and high-affinity integrins, subject to mechanical feedback. This is incorporated into a finite-element simulation of the extravasation process, with the contractile force pulling the nucleus of the TC against elastic resistance of the ECs. To account for the interaction between the TC nucleus and the endothelium, we consider two scenarios: solid–solid contact and lubrication by cytosol. The former gives a lower bound for the required contractile force to realize transmigration, while the latter provides a more realistic representation of the process. Using physiologically reasonable parameters, our model shows that the SF and FA ensemble can produce a contractile force on the order of 70 nN, which is sufficient to deform the ECs and enable transmigration. Furthermore, we use an atomic force microscope to measure the resistant force on a human bladder cancer cell that is pushed through an endothelium cultured *in vitro*. The magnitude of the required force turns out to be in the range of 70–100 nN, comparable to the model predictions.

1. Introduction

Extravasation is a key step in metastasis of cancer. Typically, tumor cells (TCs) first exfoliate from the primary tumor, and invade the surrounding extracellular matrix (ECM) until they reach a nearby blood vessel. Through a process known as intravasation, a TC breaches the blood vessel wall to enter the blood circulation, thus becoming a circulating tumor cell (CTC) [1]. After being carried to a target tissue or organ, the CTC extravasates from the blood vessel, i.e. it forces through the endothelium and basal membrane of the blood vessel to invade the tissue outside, and establish a new colony in the target site. Although both intravasation and extravasation entail breaching the endothelial barrier of the blood vessel, the two differ significantly in the signaling pathways and physical process [2–4]. We will focus only on extravasation in this paper. As we will only deal with circulating TCs, we refer to them simply as TCs hereafter.

TCs may extravasate through three distinct mechanisms: intercalation into the endothelium, paracellular transmigration between endothelial cells (ECs) and transcellular transmigration through an EC [5]. Most cancer cells follow the paracellular route *in vitro*, although it is unclear what factors determine the preferred route of transmigration *in vivo* [3]. Henceforth we will focus on the paracellular route. Through decades of focused research, much has been learned about

the biochemical signaling that controls extravasation. For example, the adhesion to ECs is known to be controlled by cell-surface proteins such as CD44, MUC1, E-selectin, ICAM-1, VCAM-1 and integrins [5, 6]. The adhesion triggers remodeling of the cytoskeleton of the TC and formation of protrusions, through the CDC42/Rac1 pathway, activating it for deformation and transmigration [7]. Finally, the TC also signals to the ECs, causing them to soften and retract from each other and disrupting the EC junctions. This involves, among other pathways, the phosphorylation and disassembly of the VE-cadherin–β-catenin complex [8, 9], with the result of opening the EC junction to facilitate TC transmigration. A more detailed description of the signaling pathways can be found in a review by Reymond *et al* [3].

In contrast to our knowledge of the biochemical signaling, much less is known about the mechanical forces involved in extravasation. Recent development in microfluidic lab-on-chip devices has allowed *in vitro* reproduction and observation of the extravasation process. Chen *et al* [11, 12] developed assays of a highly realistic vascular network on a perfused microfluidic chip, through which cancer cells can be introduced. They are seen to extend invadopodium-like protrusions through the junctions between ECs, which then adhere to the ECM outside. Antagonizing a key integrin β1 in the TCs causes them to remain round and fail to protrude in-between the ECs, and extravasation is abolished [10]. Based on these observations, Chen *et al* [10, 11] have hypothesized the following scenario for paracellular transmigration of TCs (figure 1). First, the TC extends a protrusion through the junction between ECs. As the protrusion grows in size, it branches out at the front. As its tips reach the basement membrane outside the endothelium, activated integrins help form secure focal adhesion (FA) sites. As more of the TC body moves out through the EC constriction, the relatively rigid nucleus is left behind inside the spherical-shaped membrane. Finally, contraction of the actomyosin in the stress fibers (SFs) pulls the nucleus through the constriction to complete the extravasation. More recently, Abidine *et al* [13] reported high-resolution images of the cancer cell during transmigration, and identified rapid reorganization of TC actin below the nucleus and close to the EC junction. This seems to support the above hypothesis, especially the idea of SFs forming inside the TC protrusion.

This picture for extravasation attributes the driving force to contraction of the SFs inside the 'filopodium-like protrusions' extended from the TC [3, 14], termed *invadopodia* hereafter. But it also raises further questions. Are typical SFs capable of generating the force necessary for overcoming the resistance to the passage? How do the size of the EC opening and the rigidity of the ECM affect the balance between the driving force and the resistance? Cao *et al* [15] built a mechanical model on the transmigration of a hyperelastic TC nucleus through small constrictions. By specifying a constant force that pulls on the nucleus, an elastic equilibrium is computed where elastic resistance due to the nuclear and endothelial deformations balances the pulling force. The main result is a critical pulling force for the passage, which for the geometric and mechanical parameters adopted amounts to 38 nN. Because this is essentially a static calculation, it does not give a dynamic picture of the transmigration. In particular, although the actomyosin apparatus is modeled as under biochemical control and responsive to external deformation [16], the static nature of the computation implies that this force is essentially prescribed; the biochemical factors do not participate in the mechanical equilibrium nor influence the final result. Besides, the cell membrane and cytosol of the TC are neglected, and the nucleus is assumed to compress the EC in direct solid-solid contact.

Our model is inspired by Cao *et al* [15], and aims to test the invadopodium-based mechanism hypothesized by Chen *et al* [10]. Toward this goal, we will simulate the dynamic extravasation of a TC through the junction between ECs. It goes beyond Cao *et al*'s model in several aspects. First, we use finite elements to track the transmigration dynamically, with cell and tissue deformation, dynamic remodeling of the SFs and the FAs and the displacement of the TC occurring simultaneously in time. Second, the pulling force in the TC invadopodia is modeled by adopting Deshpande *et al*'s models [17–19] for the SFs and the FAs, both controlled by biochemical signaling with a mechanical feedback. Thus, the biochemical factors exert a direct influence on the transmigration. Finally, we include the TC cytosol and membrane in the model, in addition to the nucleus, for a more realistic representation. This allows us to probe the mechanical contact between the TC and EC.

Using realistic geometric, mechanical and biochemical parameters, our model predicts a maximum resistance to transmigration of about 70 nN. More importantly, the SF and FA assembly is predicted to be able to provide forces of this magnitude to enable extravasation. Finally, we also report experimental measurements of the force required to push a human bladder cancer cell through a HUVEC endothelium. The driving force for the transmigration turns out to be in the range of 70–100 nN, in reasonable agreement with the model predictions.

2. Methods

2.1. Problem setup

The geometric setup and the hyperelasticity of the TC and EC are modeled after Cao *et al* [15], with the TC being pulled through an axisymmetric opening in hyperelastic endothelium (figure 2). For simplicity, the model accounts for a single invadopodium, even though *in vitro* images suggest the possibility of multiple protrusions or branches [11]. In addition,

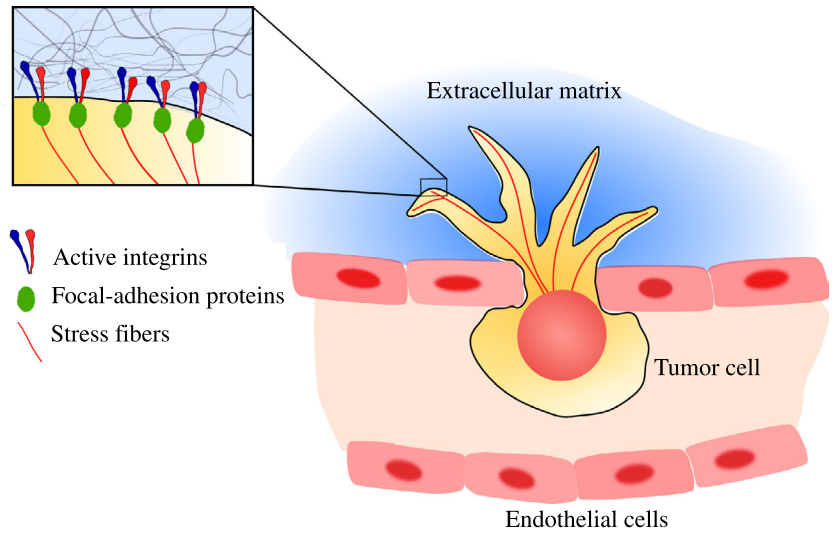

Figure 1. An invadopodium-based mechanism for extravasation proposed by Chen *et al* [10]. Inside the TC, actomyosin assembles into SFs that propel a protrusion between the ECs. Adhesion molecules, including $\alpha 3\beta 1$ and $\alpha 6\beta 1$ integrins, anchor the tips of the protrusion onto laminin of the ECM. The focal-adhesion proteins include tensin, talin and vinculin among others. Actomyosin contraction in the SFs then pulls the TC past the constriction between ECs.

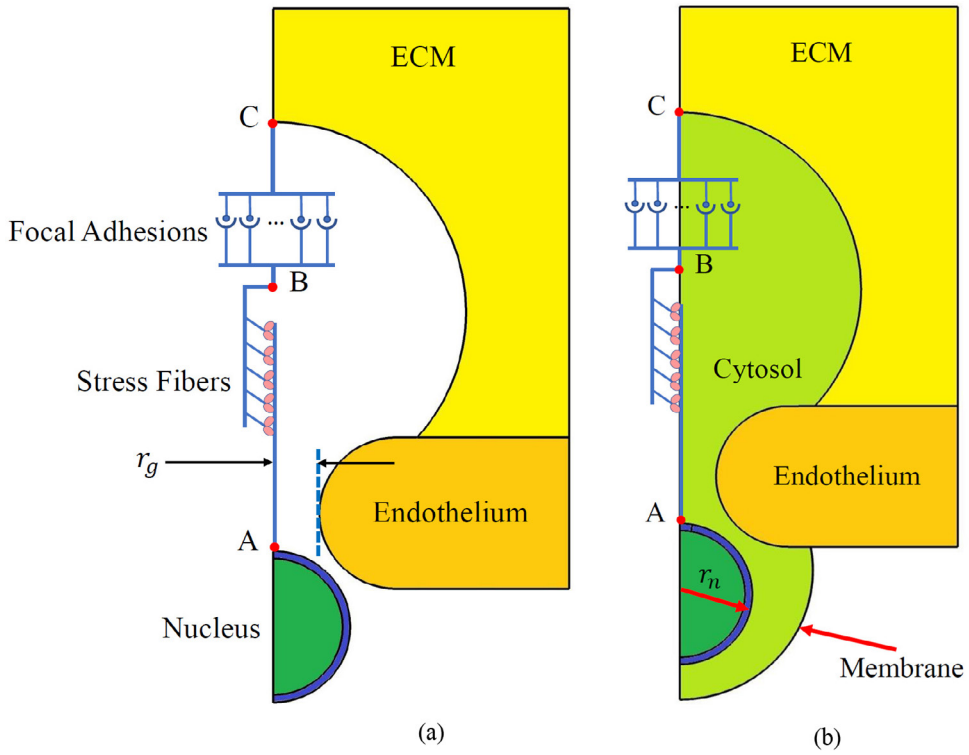

Figure 2. (a) Schematic showing the geometric setup for the 'dry-contact' simulation. SFs AB and FAs BC link the nucleus to the roof of the ECM cavity. The TC membrane and cytosol are ignored, and the critical condition of the breakthrough of the TC nucleus is determined from the direct but frictionless contact between the nucleus and the endothelium. (b) Schematic illustrating the geometric setup for the 'wet-contact' simulation, with the TC membrane and cytosol explicitly accounted for.

we have neglected any plasma flow inside the capillary, because the transmigration essays typically do not have ongoing perfusion of the vascular network [11], or because the cancer cells tend to occlude the capillary to prevent flow [20]. The opening that allows the passage appears to be small in comparison to the dimension of the TC nucleus [11, 15]. Therefore, it is reasonable to assume tight contact between the TC and EC. Given the multiple cellular components involved in the process, including the TC nucleus, cytosolic fluid and cell membrane, as well as the EC, the mechanics of contact requires a careful treatment.

In a recent model, Cao *et al* [15] have ignored the TC cytosol and membrane, and assumed direct solid-solid contact between the TC nucleus and the EC. Conceivably, the lubrication between the nucleus and the membrane [21] and between the membrane and the constriction [22] can play significant roles. In

this work, therefore, we will test two cases: the 'dry-contact' case of Cao *et al* [15] with direct solid contact between the TC nucleus and the EC (figure 2(a)), and the 'wet-contact' case that includes the cytosol and TC cell membrane (figure 2(b)). In the dry-contact simulation, the contact force is handled by a penalty method commonly used in solid-contact models [23]. In the wet-contact case, the cytosol flow within the thin gap between the TC and EC provides the lubricating pressure that prevents solid-solid contact. Including the cytosol narrows the opening available for the nucleus, and introduces additional viscous friction. So the wet contact should provide a greater resistance to the passage of the TC, and the dry contact is expected to provide the lower bound for the pulling force needed for passage. In both cases, the extravasation hinges on nuclear deformation, which is known to be a key factor in cell migration [24].

In both the dry- and wet-contact simulations, the TC has an initially round nucleus of radius r_n. The endothelium is modeled as a flat elastic layer with a circular hole of radius r_g in the middle, which is smaller than the nuclear radius r_n. Above the ECs the ECM was treated as an elastic material with a cavity in the middle. The rationale for the cavity is that cancer cells are known to create a space in the ECM either by degrading it [25] or by exploiting the tissue's plasticity [26]. The contractile apparatus of the invadopodium consists of SFs and FAs; the two are connected in series with the nucleus at one end and the ECM at the other. In the wet-contact simulations, we assume that the cavity is filled with the cytosol of the TC, its membrane being in contact with the ECM. We have in general a fluid-structure interaction problem, with partial differential equations to be solved for the cytosol fluid flow and the elastic deformation of various elastic components—the ECM, EC and TC nucleus and membrane. Besides, the SF-FA assembly evolves temporally according to a set of ordinary differential equations. The dry-contact case lacks the fluid flow and fluid-structure interaction, and is therefore simpler.

The governing equations are solved, together with proper boundary conditions, by using COMSOL Multiphysics, a finite-element package. See online supplemental information (SI) (stacks.iop.org/Phys-Bio/17/036004/mmedia), section 1 for the complete set of governing equation and the boundary conditions, as well as a description of the geometric setup and the numerical techniques. All the model parameters are summarized in section 2 of the SI, along with brief discussions of their evaluation and sources. A few key components of the methodology are described below.

2.2. Chemomechanics of the SFs and FAs

Connecting the TC nucleus to the ceiling of the cavity is an assembly of SFs and FAs in series. The SF contraction promotes the stabilization and growth of the FA [27]. Together, the assembly exerts a force on the top of the nucleus and pulls the nucleus and the whole cell through the narrow constriction against the elastic resistance due to the deformation of the nucleus and the endothelium. To represent the coupled dynamics of the SF and FA, we adapt the models of Deshpande *et al* for the SF contractility and FA growth [17, 19]. In the original model, the FA is being sheared with force and strain tangential to the substrate. In our setup, FA is being stretched by the SF, with force and strain perpendicular to the substrate. The adapted model can predict stiffness-dependent actomyosin force generation and FA formation due to the normal force on integrins.

The state of the SFs is represented by the fraction of activated myosin motors η on the SF, which ranges from 0 to 1. The kinetics of η depends on activation by an external signal (e.g. an influx of Ca^{2+} ions [18]) and force-regulated deactivation:

$$\frac{d\eta}{dt} = (1-\eta)k_a e^{-\frac{t}{\theta}} - k_d\left(\eta - \frac{\tau}{\tau_{max}}\right), \qquad (1)$$

where k_a and k_d are the kinetic rates for myosin activation and deactivation, $e^{-t/\theta}$ represents an exponentially decaying calcium signal [17, 18], and the deactivation is suppressed by the tension τ in a well-documented positive feedback [28, 29], τ_{max} being the maximum tension when the myosin is fully activated ($\eta = 1$). Since the SF is under *tension* as a result of actomyosin *contraction*, the terms 'tension' and 'contractile force' are synonyms in the current context. The kinetic equation above is complemented by a constitutive equation for the SF, relating the tension τ by a Hill-like function to the contraction or extension rate of the SFs v_f, similar to force generation in muscle cells [17, 18]:

$$\tau = \begin{cases} 0, & \frac{v_f}{v_0} < -\frac{\eta}{k_v}, \\ \eta\tau_{max}\left(1 + \frac{k_v}{\eta}\frac{v_f}{v_0}\right), & -\frac{\eta}{k_v} \leqslant \frac{v_f}{v_0} \leqslant 0, \\ \eta\tau_{max}, & \frac{v_f}{v_0} > 0, \end{cases} \qquad (2)$$

where $v_f < 0$ signifies contraction, v_0 is the zero-load speed of a myosin motor [30] and k_v is the fractional contraction rate at which the SFs can no longer sustain a tension [18]. The FA dynamics are governed by the conversion from low-affinity integrins to high-affinity integrins that can bond to the ECM. The integrin-ligand tension F_b shifts the thermodynamic equilibrium between the two in favor of the high-affinity integrins and FA growth [19, 31, 32]:

$$k_B T \ln\frac{\xi_H}{\xi_L} = \mu_L - \mu_H - \Phi + F_b\, d_b, \qquad (3)$$

where k_B is the Boltzmann constant, T is temperature, and ξ_H and ξ_L are the high- and low-affinity integrins per unit area, with the total number of integrins $\xi_H + \xi_L = \xi_0$ being conserved. μ_L and μ_H are the reference chemical potentials for the low- and high-affinity integrins. Φ, the stretch energy stored in each integrin bond, is a piecewise quadratic function of the

bond extension d_b, and $F_b = \partial\Phi/\partial d_b$ is the tension in each bond, which adds up to yield the total tension τ in the SF:

$$\tau = \xi_H F_b A_b, \tag{4}$$

where A_b is the area of the FA. The algebraic expressions for Φ and F_b are given in the SI. Finally, the FA and SF are also constrained geometrically by this kinematic relation:

$$v_A + v_f + v_b = v_C, \tag{5}$$

where $v_b = d(d_b)/dt$ is the rate of extension of the FA bonds, and v_A and v_C are, respectively, the velocity at the upper surface of the nucleus (point A in figure 2) and that of the ECM at the base of the FA (C in figure 2). We refer the reader to the SI and the literature [17–19] for more details of the coupled SF-FA model.

2.3. Hyperelasticity

The mechanics of the process involves elastic deformation and fluid flow, and we will formulate it as a fluid-structure interaction problem. The model setup involves four different elastic components: the TC cell membrane, the TC nucleus, the EC, and the ECM. Since the upper part of the membrane that has already exited the blood vessel is in direct contact with the ECM, we need not separately model this part of the membrane and will treat it as part of the ECM. Thus, the cytosol is in direct contact with the ECM in this upper 'dome' (see figure 2(b)). The lower part of the membrane, inside the blood vessel, is modeled as a hyperelastic material obeying the neo-Hookean constitutive equation:

$$\boldsymbol{\sigma} = GJ^{-\frac{3}{5}}\left(\boldsymbol{F}\boldsymbol{F}^T - \frac{\boldsymbol{I}}{3}\mathrm{tr}(\boldsymbol{F}\boldsymbol{F}^T)\right) - K(J-1), \tag{6}$$

where $F_{ij} = \partial x_i/\partial X_j$ is the deformation gradient tensor, with $\boldsymbol{X}$ and $\boldsymbol{x}$ being the undeformed and current positions of a material point, and $J = \det \boldsymbol{F}$. The coefficients G and K are the shear and bulk modulus, respectively, connected via the Poisson ratio ν: $K = \frac{2G}{3}\frac{1+\nu}{1-2\nu}$. The upper end of the TC membrane is attached onto the endothelium, and geometric details can be found in section 1 of the SI.

The cell nucleus contains a large quantity of water and is a poroelastic material. Following [15], however, we will treat it as a heterogeneous neo-Hookean material with a soft core of radius $r_c = 2.7\ \mu$m and a more rigid shell of thickness $\delta = 0.3\ \mu$m. The permeation of water can be shown to occur at a much shorter time scale than the extravasation, and can thus be ignored [15]. The shear and bulk moduli of the shell are 10 times those of the core. Moreover, the EC and the ECM are both taken to be neo-Hookean solids. The moduli of all the elastic components are given in section 2 of the SI. Finally, in all the hyperelastic bodies, the governing equation for solving for mechanical deformation is given by:

$$\nabla \cdot \boldsymbol{\sigma} = 0. \tag{7}$$

2.4. Cytosolic fluid dynamics

We treat the cytosol as a viscous Newtonian fluid, and model its flow by the Navier–Stokes equations:

$$\nabla \cdot \boldsymbol{v} = 0, \tag{8}$$

$$\rho\left(\frac{\partial \boldsymbol{v}}{\partial t} + \boldsymbol{v}\cdot\nabla\boldsymbol{v}\right) = -\nabla p + \mu\nabla^2\boldsymbol{v}, \tag{9}$$

where p is pressure, $\boldsymbol{v}$ is the velocity vector, ρ is the density of the cytosol and μ is a constant cytosolic viscosity. Aside from the viscous cytosol, the nucleus may experience additional drag due to factors not accounted for in our model, e.g. contact and interference by nearby ECM or basal membrane [10, 11], adhesion to nearby substrate [33], and interaction with the various cytoskeletal filaments in contact with the nucleus, especially the intermediate filaments that form scaffolds for the nucleus [34, 35]. To account for this additional drag, we impose a distributed 'Darcy-like' drag on the surface of the nucleus, in the form of $-\kappa\boldsymbol{v}$, proportional and opposite in direction to the local velocity on the nuclear surface. This drag force is distributed among the surface nodes on the TC nucleus in the form of a surface traction. The traction then enters the elastic deformation of the nucleus as a boundary force. The drag coefficient κ is chosen so that the nucleus attains a velocity during extravasation that is comparable to experimental observations. See section 2 of SI for further discussion.

Thus, the model comprises interconnected chemo-mechanical factors as described in the preceding subsections. They can be graphically represented by the schematic in figure 3.

2.5. Experimental techniques

The aim of the experiment is to measure the forces involved in the transmigration of a cancer cell in an *in vitro* extravasation assay. As the invadopodium is surrounded by the endothelium on the side, and sandwiched by the TC and the ECM on both ends, it is difficult to access. Thus we have no easy way of measuring the pulling force on the invadopodium directly. This has led us to a different strategy, by pushing a fixed TC through an EC junction by using the tip of the cantilever of an atomic force microscope (AFM). Assuming zero inertia, the pushing force by the AFM cantilever must balance the elastic resistance exerted by the EC on the TC. Similarly, during extravasation, the tension in the invadopodium must balance the elastic resistance by the EC. Assuming equal elastic resistance in both cases, we can equate the pushing force on the AFM cantilever to the tensile force in the invadopodium during actual extravasation. Then we can determine if the measured force is

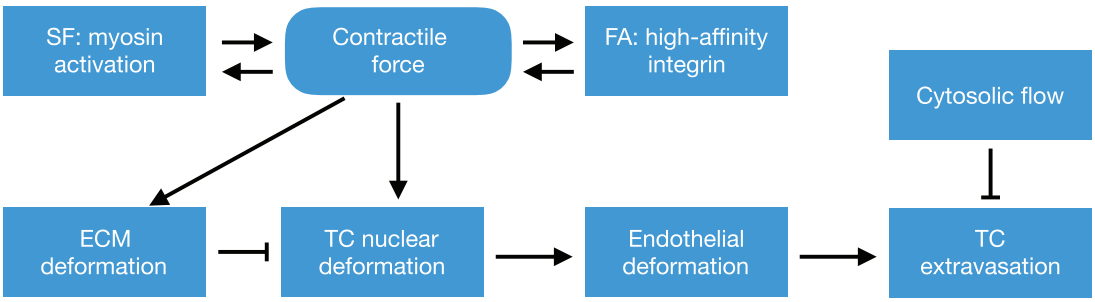

Figure 3. Schematic showing the various components of the model. A pointed arrowhead means 'activate' or 'promote' whereas a flat arrowhead means 'impede' or 'inhibit'.

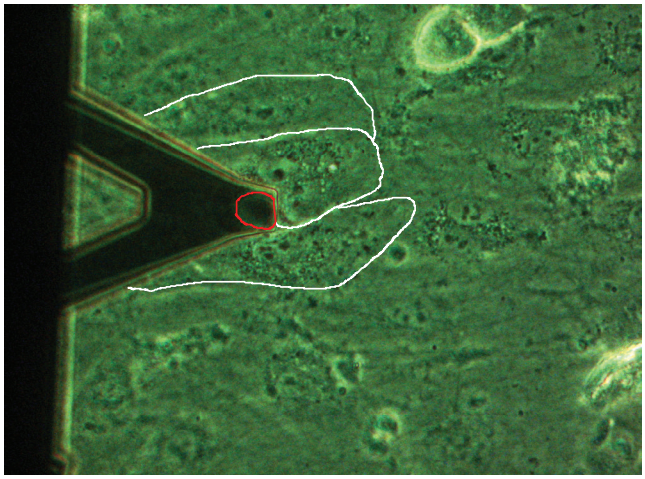

Figure 4. Phase contrast image shows a T24 cancer cell attached onto a V-shaped cantilever in contact with the HUVEC monolayer. The T24 cell contour is shown in red and the outlines of several neighboring ECs are drawn in white. As a length scale, the diameter of the cancer cell is roughly 17 μm. The image is taken from below the endothelium, which is transparent.

consistent with those predicted by the dry-contact and wet-contact simulations.

Experiments were performed using a Nanowizard II Atomic Force Microscope (JPK Instruments, Berlin, Germany) mounted on an inverted microscope (Observer D1, Zeiss, AG). We used tipless cantilevers (MLCT, Bruker, Camarillo, CA) with a nominal spring constant k $\sim$ 0.6 N m^{-1}, calibrated using the thermal noise method [36]. A T24 invasive bladder carcinoma cancer cell [13] was attached to the tipless cantilever using a pre-established protocol [37, 38]. The attached cell was fixed using 4% Paraformaldehyde followed by 96% alcohol, before it had time to spread, then it was rinsed in phosphate buffered saline thrice. Eventually the cell exhibited a round shape with a diameter of roughly 17 μm (see figure 4).

Human umbilical vein ECs (HUVECs) were cultured in cell culture medium for ECs (PromoCell, Heidelberg, Germany) supplemented with antibiotics. ECs at passages P2–P4 were grown on a collagen gel (thickness $\sim$100 μm, 8 mg ml^{-1}) in a Petri dish adapted for microscopy, until confluence was reached. The Petri dish was mounted on the AFM, and the cantilever with fixed T24 cell was lowered down until contact was made precisely at a HUVEC junction (figure 4). Then gradual indentation was achieved, either manually by 1 μm steps or continuously at a constant velocity of 0.01 μm s^{-1} or 0.05 μm s^{-1}. To evaluate the collagen deformation and stiffness, a control experiment was carried out with the same fixed T24 cell but without HUVECs to deform the collagen layer.

The forcing on the AFM tip can be measured down to pico-Newton accuracy, and we can generate a force-displacement curve from the indentation experiment. The point of passage is ascertained by two criteria. The first is a leveling-off of the force with increasing displacement of the TC, indicating a maximum resistance. The second is a geometric criterion of the displacement reaching the radius of the TC. Data presented in the next section will show how these two criteria roughly concur.

3. Results

To test the invadopodium-based hypothesis of cancer cell transmigration, we seek to answer the following question: what conditions determine whether a TC succeeds in extravasation? This depends on whether the active driving force generated in the SF-FA machinery is able to deform the TC and the EC sufficiently to allow the passage of the TC. We will first test the dry-contact scenario and then the wet-contact

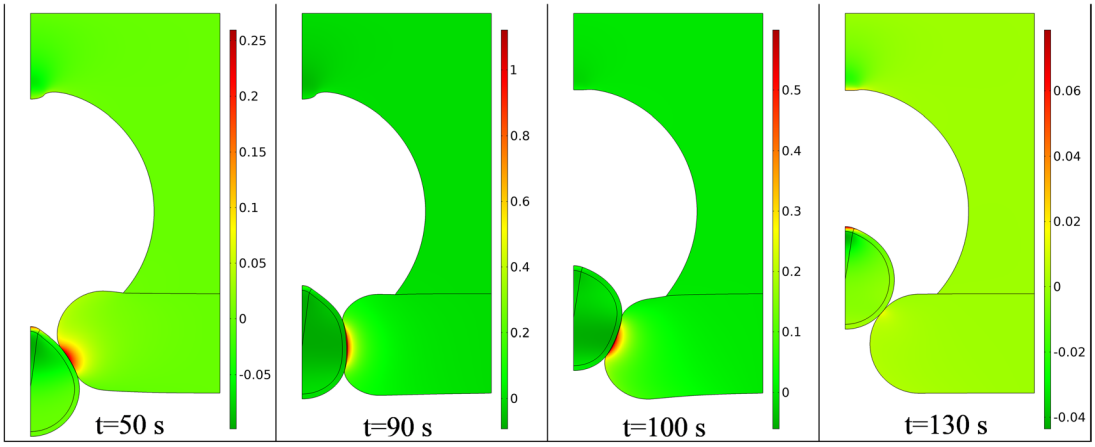

Figure 5. Snapshots showing the progression of transmigration in the dry-contact setup of the simulation. The color contours show the local strain in the vertical direction.

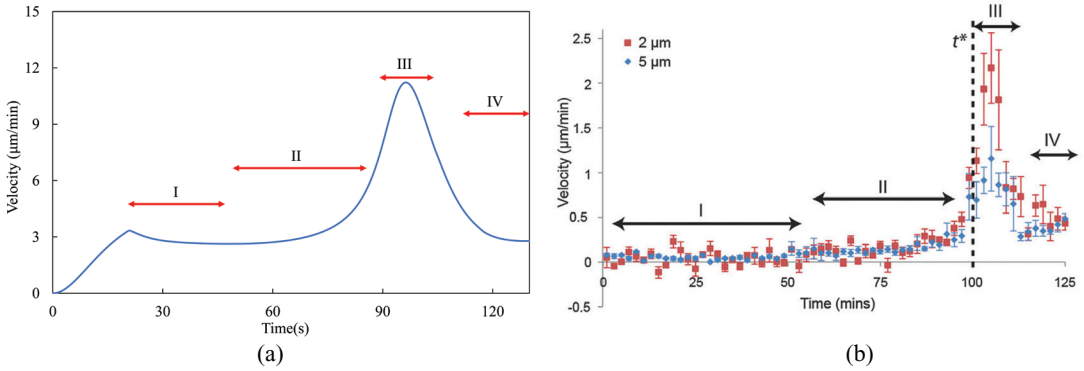

Figure 6. Comparison of the nucleus velocity v_n during the passage between (a) our model prediction and (b) the experimental measurement of [33], with the two symbols indicating two data sets for different gap sizes. Adapted from [33] with permission, © Oxford University Press.

scenario. The results presented below correspond to the baseline parameter set described in the SI.

3.1. Dry contact simulation

Figure 5 shows a time sequence of snapshots illustrating how the nucleus is pulled through the narrow opening in the endothelium by the SF. The endothelial opening has a radius $r_g = 1.5$ μm in the middle, while the TC nucleus has an undeformed radius $r_n = 3$ μm, twice the size of the opening. First, we initiate the calcium signal to trigger the myosin activation. This produces tension in the SF that pulls the TC nucleus toward the gap in the TC. Since the nucleus has an undeformed size that is bigger than the gap size, it stalls and comes into solid-solid contact with the surface of the EC ($t = 50$ s). In the contact zone, there is a normal contact force but no tangential friction. Under the pulling force by the SF, the nucleus, EC and the ECM continue to deform elastically until $t = 90$ s, when the nucleus is approaching the narrowest part of the EC constriction. Since the nuclear shell is much more rigid than the EC [15], it deforms much less in this process. Then a breakthrough happens as the nucleus transmigrates successfully ($t = 100$ s). Note that at this instant, the normal force from the EC propels the TC nucleus forward. The transmigration is completed by $t = 130$ s. The process is depicted in Movie 1 in the SI.

Figure 6(a) shows the evolution of the velocity v_n of the centroid of the nucleus during its transmigration. Upon start of the simulation, the velocity rises till $t \approx 20$ s. This acceleration is owing to the geometric setup that puts an initial clearance between the tumor nucleus and the endothelium, and is not an intrinsic part of the physics. Afterwards, the nuclear velocity exhibits four distinct phases as demarcated in the graph. First, the nucleus movement is impeded after it makes contact with the endothelial surface, and the velocity declines. Second, the nucleus and the EC deform as the SF contracts more, and v_n slowly accelerates. Third, the nucleus snaps through the gap, with a sharp rise in v_n followed by a sharp decline. The acceleration is partly due to the release of stored elastic energy in the nucleus and the EC after the breakthrough; this is visible in the snapshot for $t = 100$ s in figure 5. The deceleration after breakthrough reflects the decline in the tensile force on a rapidly shortening

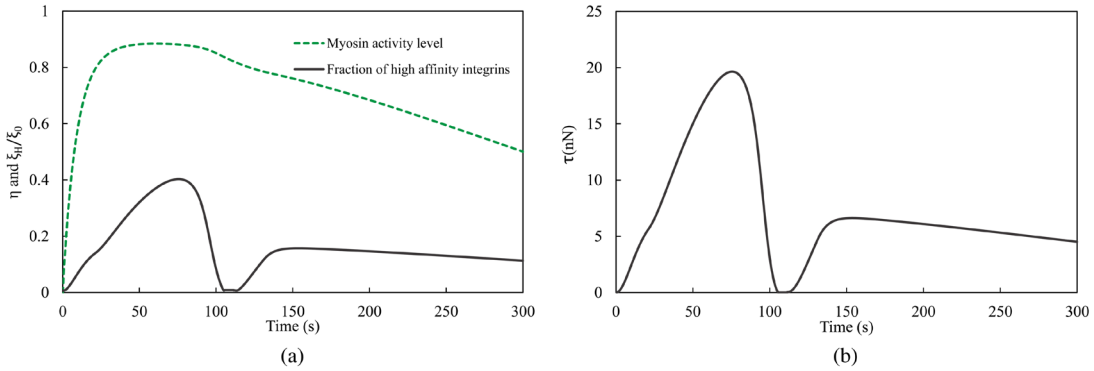

Figure 7. Dynamics of transmigration illustrated by the evolution of (a) the active myosin level in the SF η and the fraction of high-affinity integrins ξ_H/ξ_0 in the FA; (b) the tension τ in the SF.

SF. Finally, the nucleus settles down to a small velocity, as the SF gradually disassembles following the loss of tension.

We can compare the model prediction with experimental observations of Davidson *et al* [33] (figure 6(b)). The simulation has captured the qualitative features of the experiment, including the four phases in the variation of the nuclear velocity. However, the time scale and the peak velocity are quite different. Our model predicts a transit time of roughly 2 min, compared with the experimental value of over 100 min. A possible explanation for the difference is that the experiment is based on the crawling of a fibroblast through narrow constrictions due to the gradient of chemoattractant, which is a slow process determined by the biochemical rates of chemotaxis. In contrast, the breakthrough of nucleus during extravasation is governed by the much faster dynamics of SF contraction.

During the transmigration, the active myosin level η, the fraction of high-affinity integrins ξ_H/ξ_0 in the FA and the contractile force τ in the SF follow similar trajectories of temporal evolution (figure 7). According to equation (1), the calcium signal prompts the rapid assembly of the actomyosin SFs . In the meantime, the myosin deactivation also rises with η, the balance between the two resulting in a plateauing of η around $t = 50$ s. After η plateaus, the SF tension τ continues to grow because of the 'viscous' v_f/v_0 term in the constitutive equation (equation (2)). The nucleus coming into contact with the EC, its motion slows down as does the rate of SF contraction v_f, thus raising τ. The rising tension also drives the continual rise of the high-affinity integrins ξ_H (equation (3)), which amounts to a growth of the FA in a well-documented positive feedback [31]. As the nucleus snaps through the passage ($90 < t < 100$ s in figure 5), its sudden acceleration leads to a large negative v_f, and consequently a sudden drop in the contractile force τ from a peak of about 20 nN toward zero according to the SF constitutive equation (equation (2)). As a consequence, the actomyosin SF disassembles quickly and η declines, and the FA weakens with declining high-affinity integrins ξ_H. Later, as the nucleus decelerates quickly, the SF contraction speed v_f declines and the tension τ recovers somewhat (see equation (2)) before decaying slowly over a long time. The same pattern is mirrored by ξ_H.

In section 3 of the SI, we have included a parametric study that shows how the success of the extravasation depends on model parameters such as the size of the EC opening, ECM modulus, and duration of the decaying signal that stimulates myosin activation.

3.2. Wet-contact simulation

The wet-contact simulations include the effects of the cytosol and the TC membrane. The cytosol affects the translocation of the nucleus both geometrically and hydrodynamically. Geometrically, a film of cytosol that cushions the nucleus from the endothelium effectively narrows the space available for the nucleus, and thus hinders extravasation. Hydrodynamically, the cytosol film acts like a lubricating layer, producing a viscous friction and a lubricating pressure between the nucleus and the endothelium, in place of the solid contact force in the dry-contact situation. Since the dry-contact model is frictionless, the viscous friction probably also increases the resistance to extravasation for the wet-contact model. Finally, having the cytosol inside the membrane also allows the model to account for the 'back pressure', i.e. the pressure difference between the fluid ahead of the nucleus and behind it, a potentially important effect [15]. Should the contractile force fail to pull the nucleus through the gap, it will slowly pull the nucleus against the membrane toward a static state where the nucleus, TC membrane and the EC outside are in solid contact. In this sense, the dry-contact force computed in the previous subsection should provide a lower bound for the contractile force that is required for extravasation.

Figure 8 shows snapshots during passage of the nucleus through the opening in the endothelium. The color scale in the solid indicates the strain component in the vertical direction, while that in the cytosol marks the magnitude of the velocity. As the SFs pull the nucleus into the narrow gap ($t = 60$ s), not only does the nucleus deform and stretch in the vertical direction, so do the EC and the ECM. The deformation in

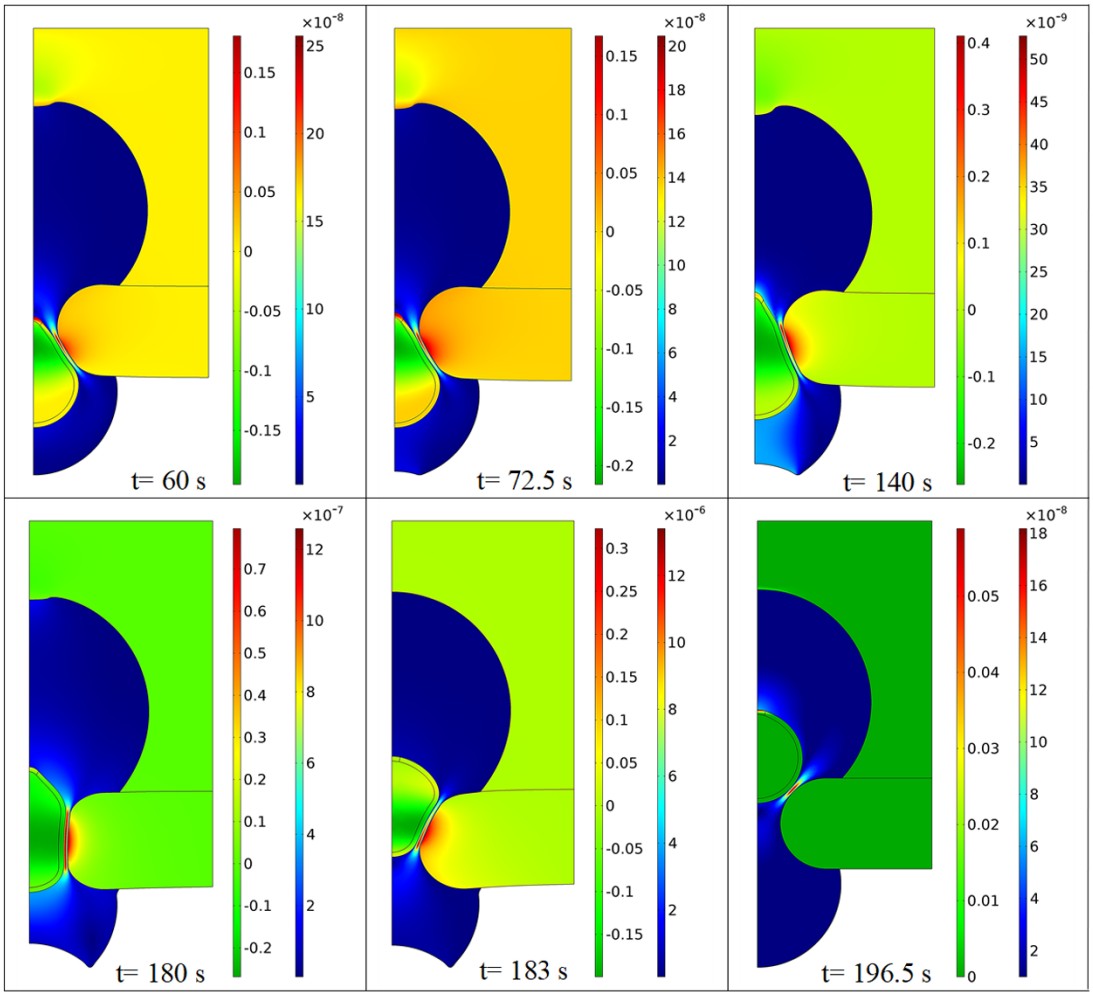

Figure 8. Snapshots illustrating the extravasation of a tumor-cell nucleus in a wet-contact simulation. The left color bar shows the level of the vertical strain component in the solids while the right color bar shows the velocity magnitude (m/s) in the cytosol.

the ECM directly above the nucleus is caused by the pulling force in the SF and the FA. Meanwhile the cytosol is squeezed in the upper chamber, where the pressure rises and pumps the cytosol downward through the gap (figures S6 and S7 in the SI). Later ($t = 72.5$ s), the upward movement of the nucleus has generated such a low pressure underneath that the cell membrane caves in at the bottom. This concave shape may be partly due to the model's neglecting the cortical tension. It is unclear whether such change of shape occurs during extravasation *in vitro* or *in vivo*. The greatest amount of nuclear deformation occurs at $t = 180$ s. Once the centroid of the nucleus is past the narrowest point of the gap ($t = 183$ s), the elastic resistance on the nucleus drops suddenly. In fact, the relaxation of the deformed EC now provides an upward pushing force on the nucleus. As a result, the tension on the SFs drops quickly, while the ceiling of the ECM relaxes as well. The passage is complete by $t = 196.5$ s. An animation of the extravasation can be viewed in Movie 2 of the SI. The transient cytosolic flow turns out to be highly intricate during the nuclear passage, and is analyzed in section 4 of the SI. Ultimately, the back pressure and viscous friction due to the cytosolic flow are negligibly small. The cytosol influences the passage of the TC nucleus mostly by the lubrication film occupying space and transmitting pressure between the nucleus and the EC.

Similar to the dry-contact case, the wet-contact transmigration can be analyzed more quantitatively through the temporal evolution of the nuclear velocity v_n, the myosin activation η and tension τ in the SF, and the high-affinity integrins ξ_H in the FA. The nuclear velocity v_n, depicted in figure 9, exhibits the same four phases as in figure 6. But the wet-contact case takes much longer in phase I; there is a long period (roughly from $t = 20$ s to 120 s) in which the nucleus decelerates slowly. This is evidently due to the lubricating flow in the thin film between nucleus and the EC. Subsequently, the acceleration phase II and breakthrough phase III take roughly the same time as in the dry-contact case. During the breakthrough, the nucleus attains a much higher velocity (maximum of 45 μm min^{-1}, almost four times that for the dry-contact case).

The evolution of η, τ and ξ_H in figure 10 resembles that of the dry-contact case in figure 7, with some interesting quantitative differences. Although the myosin activation η saturates at more or less the same

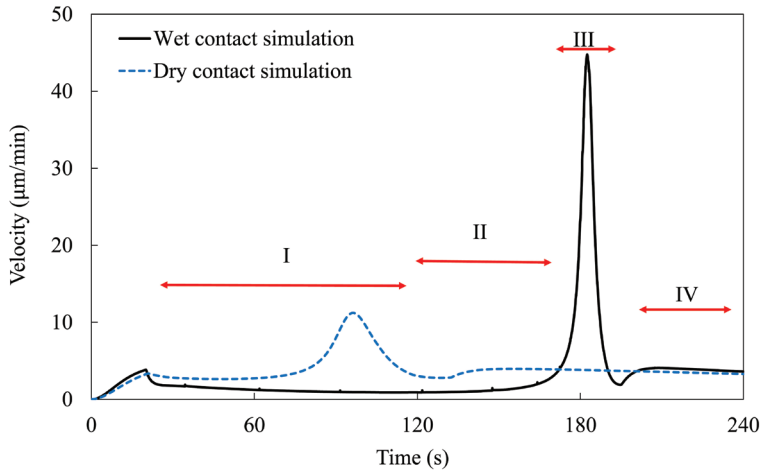

Figure 9. Dynamics of transmigration illustrated by the temporal evolution of the velocity of the centroid of the nucleus in time. The dry-contact result is also shown for comparison.

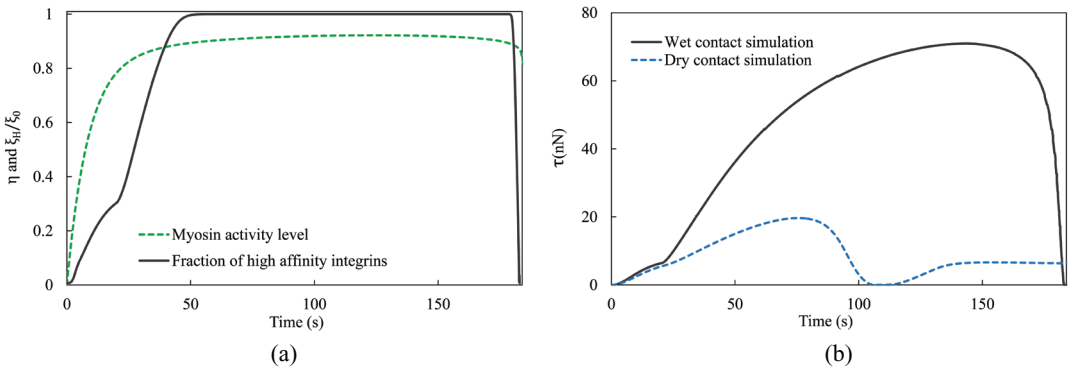

Figure 10. The temporal evolution of (a) the active myosin level η on the SFs and the fraction of high-affinity integrin ξ_H/ξ_0 in the FAs; (b) the tension τ on the SFs. The force for the dry-contact case is also shown for comparison. In later times ($t > 200$ s), τ and ξ_H recover somewhat as in the dry-contact case, but this portion of the evolution is omitted for a better view.

level, the tension τ rises to much larger magnitude in the wet-contact simulation. The presence of the cytosol narrows the space available for the nucleus to pass, and also adds a viscous friction against the passage. Thus the nucleus encounters stronger initial resistance and moves up more slowly as the nucleus deforms gradually. This explains the long deceleration phase II of figure 9. Through the constitutive equation of the SF (equation (2)), the decelerating SF contraction rate allows τ to continue to rise after η has saturated. This is also the cause of the upturn in τ at $t = 20$ s when the nucleus initially encounters resistance in the gap and decelerates sharply. Through the stress-feedback mechanism in the FA, the rising τ raises ξ_H. In fact, the tension is so strong that the fraction ξ_H/ξ_0 reaches 1 at $t \approx 50$ s, signifying complete conversion to high-affinity integrins, and stays at 1 until the extravasation completes. The breakthrough around $t = 180$ s is accompanied by a sharp peak in the nuclear velocity and a precipitous decline in the SF tension and high-affinity integrin level. The actomyosin SFs also start to disassemble. Afterwards, the nuclear velocity is largely determined by the 'Darcy-like' drag coefficient. The maximum tension in the SF over the entire process is about 70 nN.

In comparing the wet-contact and dry-contact simulations, one notes similar temporal dynamics in the SF-FA assembly, based on two positive feedbacks between the tension τ and actomyosin activation η on the one hand, and between τ and the FA strength ξ_H on the other. As anticipated in section 2.1, the wet-contact mode incurs more intense dynamics. The resistance to nuclear passage is greater, and the SF develops a stronger tension τ, accompanied by a higher level of myosin activation η and FA development ξ_H. The wet-contact model predicts a transit time of roughly 4 min, on the same order as *in vitro* observations of TC extravasation (10–15 min) [11, 13].

Our model has predicted successful extravasation in both the dry-contact and the wet-contact setup using a set of realistic parameters. The contractile device in the SF-FA assembly is able to generate the force required to deform the TC and the endothelium sufficiently to allow transmigration. This supports the hypothesis of Chen *et al* [10, 11] that the TC uses contractile forces inside an invadopodium to pull the

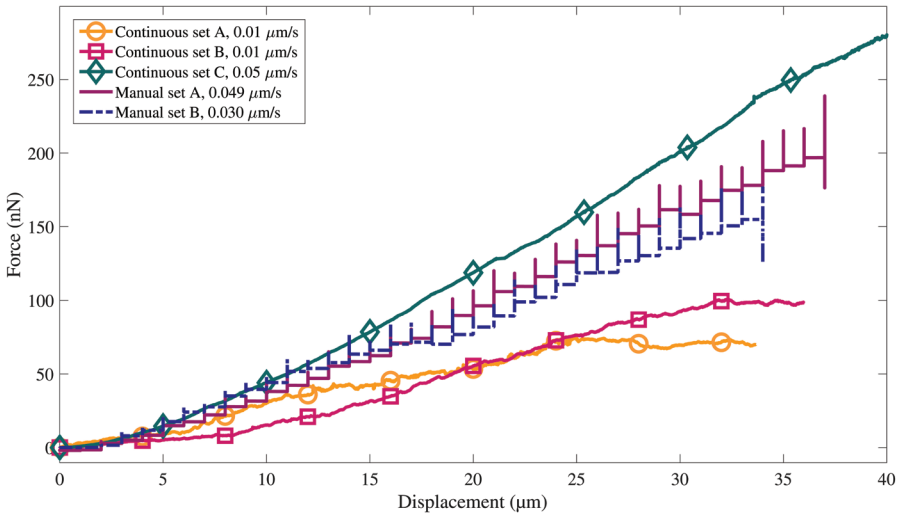

Figure 11. Experimentally measured indentation force as a function of the displacement of the fixed TC. The three relatively smooth curves with symbols are recorded in the continuous mode at two different cantilever speeds, while the two data sets with vertical spikes are measured in the manual mode.

nucleus through the narrow gap between neighboring ECs. Most interestingly, the required tension for the nuclear transmigration is approximately 70 nN for wet contact and 20 nN for dry contact. These two values straddle that of 38 nN predicted by the earlier model of Cao *et al* [15]. Which more closely approximates reality will be tested by experimental measurements.

3.3. Experimental results

As an additional test for the transmigration mechanism discussed in the above, we measure the force needed to push a fixed and passive TC through an EC junction. As explained in section 2.5, this is achieved by positioning a fixed TC on top of a HUVEC junction (figure 4) and then using the AFM cantilever to press the TC into the junction. The experiment has been done in two modes. In the manual mode, we press the TC down by a 1 μm indentation and wait for 20 to 35 s for the force signal to relax. Then this is repeated until a plateau in the force is found. In the continuous mode, a long-range piezo displacement unit is used to move the cantilever downward at a prescribed constant velocity in the range of 0.01–0.05 μm s^{-1}, to a maximum vertical displacement of 40 μm. In either mode, the pressing force obtained from the cantilever deflection is recorded as a function of the vertical displacement.

Figure 11 plots five data sets, three in the continuous mode and two in the manual mode. Of the three continuous-mode curves, two are at the slow speed of 0.01 μm s^{-1} and the other is at the much higher speed of 0.05 μm s^{-1}. The two low-speed runs yield similar data; the force initially increased with displacement, and then attains a plateau at a displacement of $z \sim 30$ μm. The plateau is taken to be an indication that the TC has entered the narrowest part of the junction and transmigration is occurring. This criterion is based on the assumption of a monotonic relationship between the elastic deformation of the HUVEC layer and its elastic resistance of the TC. As the deformation increases initially, plateaus and eventually falls as the TC passes through the junction, so should the resistance force. The plateau force is roughly 70 nN and 100 nN for the continuous data sets A and B, respectively.

An additional argument for the onset of transmigration comes from the magnitude of the displacement. We have done auxiliary experiments to measure the modulus of the collagen underlying the EC layer, by pressing a fixed TC directly onto the collagen gel layer. Such measurements have yielded an estimation of a collagen modulus of about 400 Pa. Computations using the proper thickness and modulus of the EC and collagen layers suggest that, when the TC is moved downward by a certain displacement z, about 2/3 of it is absorbed by deformation of the collagen layer, and 1/3 by the displacement of the TC relative to the EC junction. This implies that at the displacement of the force plateau, $z \sim 30$ μm, the TC should have moved about 10 μm relative to the EC junction, about 1.2 times of the TC radius (8.5 μm). Geometrically, it is reasonable that this amount of displacement corresponds to the transmigration.

The high-speed (0.05 μm s^{-1}) run in the continuous mode shows a distinct behavior, with the force increasing apparently without bound until the maximum strain tested ($z = 36$ μm). Our interpretation of this behavior is that when the TC moves at a high speed, it does not give the HUVEC cells enough time for remodeling and relaxing, which is an integral part for cancer cell extravasation [3]. As a result, transmigration never happened in this high-speed indentation experiment.

This interpretation is supported by the two data sets obtained in the manual mode. First, note that

at each fixed displacement, there is a series of force values forming a vertical cluster in the graph. This corresponds to the force relaxing as the EC remodels and softens while the TC is held at a fixed z. Second, if we divide the final displacement by the total duration of the experiment, we arrive at an average speed of 0.049 μm s^{-1} for the manual data set A and 0.030 μm s^{-1} for set B. These two speeds fall between the high-speed and low-speed continuous runs, as do the forces of the two manual runs. This suggests that the waiting time after each manual displacement was not long enough to allow full EC remodeling, and as a result we ended up with greater forces than the slower-speed continuous tests. This is consistent with the interpretation of the high-speed (0.05 μm s^{-1}) run in the continuous mode. Finally, the two manual data sets each show an apparent plateau at the end of the runs, at a maximum displacement of $z = 34$–37 μm. This may correspond to the onset of transmigration, albeit at an elevated force for the lack of sufficient EC remodeling and relaxation.

To summarize the experimental results, we take the quasi-static measurements, at the smaller constant velocity of 0.01 μm s^{-1} in the continuous mode, to correspond properly to the extravasation process where the EC cells have time to remodel sufficiently. Furthermore, we identify the plateau in the force-displacement curve with the onset of TC transmigration, and the plateau force $F = 70$–100 nN to be the required driving force. This range is consistent with our model prediction of a required tension of $F = 70$ nN in figure 10(b), and the experimental results seem compatible with the model predictions.

4. Discussion and conclusion

In this work, we have built a biomechanical model for the trans-endothelial migration of a TC during extravasation, with the aim of testing a hypothesis proposed by Chen *et al* [10, 11] that the transmigration is driven by the contractile force in the invadopodium protruding from the cancer cell to the ECM outside the endothelium. The model integrates several components into a coherent framework: the elastic deformation of the tumor and ECs and the ECM, the fluid flow inside the TC cytosol, and the coupled dynamics of the SFs inside the invadopodium and the FAs. Using a set of parameters chosen to approximate a realistic extravasation, the model predicts successful transmigration of the TC. Besides, we have also measured experimentally the resistance force experienced by a TC as it is pushed through an endothelial junction *in vitro*. The main results of the work can be summarized as follows:

- Triggered by an external signal such as an influx of calcium ions, the SF assembles and grows simultaneously with the FA, thanks to a positive feedback between the tension and actomyosin activation, and another between the tension and growth of the FAs through growing high-affinity integrins.
- Driven by the tension in the SF-FA assembly, the TC nucleus deforms as it enters a prescribed gap representing an endothelial junction. In the meantime, the ECs and the ECM also deform until a critical point when the TC passes through the gap to extravasate.
- The measured resistance force, in the range of 70–100 nN, is consistent with model predictions of a required driving force of 70 nN. A simpler 'dry-contact' model, which ignores the TC cytosol and membrane and assumes solid-solid contact between the TC nucleus and the endothelium, under-predicts this force grossly.

These results support the invadopodium-based mechanism for the extravasation hypothesized by Chen *et al* [10, 11]. Quantitatively, the invadopodium is able to generate the force required to pull the TC through a narrow opening in the endothelial layer. Besides, the comparison between the model predictions, using both the dry-contact and the wet-contact setups, with the experimental data demonstrates the need to account for the cytosol and membrane of the TCs. Otherwise, a dry-contact model would incorrectly predict transmigration at driving forces that are too low by a factor of about 3.5.

We must emphasize the limitations of this work as well. Extravasation of TCs is a highly complex process, with multiple biochemical and mechanical factors at work. Of necessity some of these are neglected in the modeling. Perhaps the most important of these is the remodeling of the endothelium, which can be through mechanical [39] and biochemical pathways [3]. Mechanically, ECs have long been known to exhibit viscoelasticity [40], and our own experiment reported here suggests relaxation under compression. Stretching and fluid-induced shear stresses not only remodel the cytoskeleton of ECs [39, 41] but also the cell-cell junctions [42]. Biochemically, cancer cells promote SF assembly and actomyosin contraction inside ECs through the Rho pathway, causing retraction of the ECs and opening of their junctions, both facilitating the passage of the TC [8, 43, 44]. They can also directly attack the EC junctions by disrupting the VE-cadherin complex [3, 9, 45]. To a limited degree, our experiment has probed such EC remodeling under purely mechanical cues from the TC. Although the fixed TC sends no biochemical signals to the EC, its indentation into the EC elicits an immediate jump in the reactive force, which partially relaxes over a time scale of 20 to 30 seconds (see figure 11). Following this argument, one may argue that the model's capturing the required driving force ($\sim$70 nN) is fortuitous in the sense that the dynamically changing mechanical properties of the endothelium must have been represented, in an averaged sense, by

an EC modulus that is soft. Other factors that have been neglected from the model include the poroelasticity of the tumor-cell nucleus, the effect of the plasma flow inside the blood vessel, and the dynamic process of the proteolysis of the ECM.

Another potentially important omission is the biochemical pathways for actomyosin activation. This has been lumped into a simple 'activation signal' that decays exponentially in time. In reality, there exist multiple pathways for such activation, e.g. for actin polymerization through the Rac1 pathway and for myosin assembly by the RhoA pathway [18], which may add nuances to the development of the tensile force in the invadopodium.

Finally and more technically, evaluation of the model parameters has been a difficult task. For one, certain model parameters, such as the magnitudes of the activation and deactivation rates and the duration of the external signal, are not explicitly available from prior measurements, and we have adopted values from prior modeling. To partially address this uncertainty, we have reported in the SI a parametric study to map out the model predictions over a reasonable range of several key parameters. This has given us a guideline as to the applicability of the model predictions vis-à-vis a specific *in vivo* or *in vitro* extravasation process. In view of the above limitations, one should consider the model predictions in this paper a *tentative* validation of the hypothesis that we have set out to test, subject to refinement of the various model assumptions and more accurate evaluation of the parameters.

Acknowledgments

The authors acknowledge financial support by the Natural Sciences and Engineering Research Council of Canada (Discovery Grant No. 2019-04162), MITACS (Accelerate Program) and LabeX Tec 21 (Grant No. ANR-11-LABEX-0030). The computations were carried out at WestGrid (www.westgrid.ca) and Compute Canada (www.computecanada.ca). We also thank the Grenoble Nanoscience Foundation for sponsoring the AFM, Alain Duperray and Valérie M Laurent for discussions and comments on various aspects of the project, and Hamed Pouriayevali for helping with producing the graphics.

ORCID iDs

S M Amin Arefi https://orcid.org/0000-0002-8014-4738
Daria Tsvirkun https://orcid.org/0000-0002-6599-6844
Claude Verdier https://orcid.org/0000-0003-3706-7148
James J Feng https://orcid.org/0000-0002-7141-5823

References

[1] Sundling K and Lowe A 2019 Circulating tumor cells: overview and opportunities in cytology *Adv. Anat. Pathol.* **26** 56–63
[2] van Zijl F, Krupitza G and Mikulits W 2011 Initial steps of metastasis: cell invasion and endothelial transmigration *Mutat. Res. Rev. Mutat. Res.* **728** 23–34
[3] Reymond N, d'Água B B and Ridley A J 2013 Crossing the endothelial barrier during metastasis *Nat. Rev. Cancer* **13** 858–70
[4] Shenoy A K and Lu J 2016 Cancer cells remodel themselves and vasculature to overcome the endothelial barrier *Cancer Lett.* **380** 534–44
[5] Tremblay P-L, Huot J and Auger F A 2008 Mechanisms by which E-Selectin regulates diapedesis of colon cancer cells under flow conditions *Cancer Res.* **68** 5167–76
[6] Haddad O, Chotard-Ghodsnia R, Verdier C and Duperray A 2010 Tumor cell/endothelial cell tight contact upregulates endothelial adhesion molecule expression mediated by NFκB: differential role of the shear stress *Exp. Cell Res.* **316** 615–26
[7] Reymond N, Im J H, Garg R, Cox S, Soyer M, Riou P, Colomba A, Muschel R J and Ridley A J 2015 RhoC and ROCKs regulate cancer cell interactions with endothelial cells *Mol. Oncol.* **9** 1043–55
[8] Grinnell K L, Casserly B and Harrington E O 2010 Role of protein tyrosine phosphatase SHP2 in barrier function of pulmonary endothelium *Am. J. Physiol. Lung Cell. Mol. Physiol.* **298** L361–70
[9] Drabsch Y and ten Dijke P 2011 TGF-β signaling in breast cancer cell invasion and bone metastasis *J. Mammary Gland Biol. Neoplasia* **16** 97–108
[10] Chen M B, Lamar J M, Li R, Hynes R O and Kamm R D 2016 Elucidation of the roles of tumor integrin β1 in the extravasation stage of the metastasis cascade *Cancer Res.* **76** 2513–24
[11] Chen M B, Whisler J A, Jeon J S and Kamm R D 2013 Mechanisms of tumor cell extravasation in an *in vitro* microvascular network platform *Integr. Biol.* **5** 1262–71
[12] Jeon J S, Zervantonakis I K, Chung S, Kamm R D and Charest J L 2013 *In vitro* model of tumor cell extravasation *PLoS One* **8** e56910
[13] Abidine Y, Constantinescu A, Laurent V M, Rajan V S, Michel R, Laplaud V, Duperray A and Verdier C 2018 Mechanosensitivity of cancer cells in contact with soft substrates using AFM *Biophys. J.* **114** 1165–75
[14] Shibue T, Brooks M W, Inan M F, Reinhardt F and Weinberg R A 2012 The outgrowth of micrometastases is enabled by the formation of filopodium-like protrusions *Cancer Discov.* **2** 706–21
[15] Cao X, Moeendarbary E, Isermann P, Davidson P, Wang X, Chen M, Burkart A, Lammerding J, Kamm R and Shenoy V 2016 A chemomechanical model for nuclear morphology and stresses during cell transendothelial migration *Biophys. J.* **111** 1541–52
[16] Shenoy V B, Wang H and Wang X 2016 A chemo-mechanical free-energy based approach to model durotaxis and extracellular stiffness-dependent contraction and polarization of cells *Interface Focus* **6** 20150067
[17] Deshpande V S, McMeeking R M and Evans A G 2006 A bio-chemo-mechanical model for cell contractility *Proc. Natl Acad. Sci. USA* **103** 14015–20
[18] Deshpande V S, McMeeking R M and Evans A G 2007 A model for the contractility of the cytoskeleton including the effects of stress-fibre formation and dissociation *Proc. R. Soc.* A **463** 787–815
[19] Deshpande V S, Mrksich M, McMeeking R M and Evans A G 2008 A bio-mechanical model for coupling cell contractility with focal adhesion formation *J. Mech. Phys. Solids* **56** 1484–510
[20] Chen M B, Whisler J A, Fröse J, Yu C, Shin Y and Kamm R D 2017 On-chip human microvasculature assay for visualization

and quantification of tumor cell extravasation dynamics *Nat. Protoc.Protocols* **12** 865–80
[21] Caille N, Thoumine O, Tardy Y and Meister J-J 2002 Contribution of the nucleus to the mechanical properties of endothelial cells *J. Biomech.* **35** 177–87
[22] Wu T and Feng J 2015 Modeling the mechanosensitivity of neutrophils passing through a narrow-channel *Biophys. J.* **109** 2235–45
[23] Wriggers P 2006 *Computational Contact Mechanics* (Berlin: Springer)
[24] Giverso C, Grillo A and Preziosi L 2014 Influence of nucleus deformability on cell entry into cylindrical structures *Biomech. Model. Mechanobiol.* **13** 481–502
[25] Eddy R J, Weidmann M D, Sharma V P and Condeelis J S 2017 Tumor cell invadopodia: invasive protrusions that orchestrate metastasis *Trends Cell Biol.* **27** 595–607
[26] Wisdom K M *et al* 2018 Matrix mechanical plasticity regulates cancer cell migration through confining microenvironments *Nat. Commun.* **9** 4144
[27] Burridge K and Guilluy C 2016 Focal adhesions, stress fibers and mechanical tension *Exp. Cell Res.* **343** 14–20
[28] Veigel C, Molloy J E, Schmitz S and Kendrick-Jones J 2003 Load-dependent kinetics of force production by smooth muscle myosin measured with optical tweezers *Nat. Cell Biol.* **5** 980–6
[29] Kovács M, Thirumurugan K, Knight P J and Sellers J R 2007 Load-dependent mechanism of nonmuscle myosin 2 *Proc. Natl Acad. Sci. USA* **104** 9994–9
[30] Besser A and Schwarz U S 2007 Coupling biochemistry and mechanics in cell adhesion: a model for inhomogeneous stress fiber contraction *New J. Phys.* **9** 425
[31] Nicolas A, Geiger B and Safran S A 2004 Cell mechanosensitivity controls the anisotropy of focal adhesions *Proc. Natl Acad. Sci. USA* **101** 12520–5
[32] Shemesh T, Geiger B, Bershadsky A D and Kozlov M M 2005 Focal adhesions as mechanosensors: a physical mechanism *Proc. Natl Acad. Sci. USA* **102** 12383–8
[33] Davidson P M, Sliz J, Isermann P, Denais C and Lammerding J 2015 Design of a microfluidic device to quantify dynamic intra-nuclear deformation during cell migration through confining environments *Integr. Biol.* **7** 1534–46
[34] Alberts B, Johnson A, Lewis J, Raff M, Roberts K and Walter P 2007 *Molecular Biology of the Cell* 5th edn (New York: Garland Science)
[35] Kim S and Coulombe P A 2007 Intermediate filament scaffolds fulfill mechanical, organizational, and signaling functions in the cytoplasm *Genes Dev.* **21** 1581–97
[36] Butt H-J and Jaschke M 1995 Calculation of thermal noise in atomic force microscopy *Nanotechnology* **6** 1–7
[37] Laurent V M, Duperray A, Rajan V S and Verdier C 2014 Atomic force microscopy reveals a role for endothelial cell ICAM-1 expression in bladder cancer cell adherence *PLoS One* **9** e98034
[38] Rajan V S, Laurent V M, Verdier C and Duperray A 2017 Unraveling the receptor-ligand interactions between bladder cancer cells and the endothelium using AFM *Biophys. J.* **112** 1246–57
[39] Russo T, Stoll D, Nader H and Dreyfuss J 2018 Mechanical stretch implications for vascular endothelial cells: altered extracellular matrix synthesis and remodeling in pathological conditions *Life Sci.* **213** 214–25
[40] Sato M, Ohshima N and Nerem R 1996 Viscoelastic properties of cultured porcine aortic endothelial cells exposed to shear stress *J. Biomech.* **29** 461–7
[41] Osborn E A, Rabodzey A, Dewey C F and Hartwig J H 2006 Endothelial actin cytoskeleton remodeling during mechanostimulation with fluid shear stress *Am. J. Physiol. Cell Physiol.* **290** C444–52
[42] Dorland Y L and Huveneers S 2017 Cell–cell junctional mechanotransduction in endothelial remodeling *Cell. Mol. Life Sci.* **74** 279–92
[43] Li B, Zhao W-D, Tan Z-M, Fang W-G, Zhu L and Chen Y-H 2006 Involvement of Rho/ROCK signalling in small cell lung cancer migration through human brain microvascular endothelial cells *FEBS Lett.* **580** 4252–60
[44] Cain R J, Vanhaesebroeck B and Ridley A J 2010 The PI3K p110α isoform regulates endothelial adherens junctions via Pyk2 and Rac1 *J. Cell Biol.* **188** 863–76
[45] Tremblay P L, Auger F A and Huot J 2006 Regulation of transendothelial migration of colon cancer cells by E-selectin-mediated activation of p38 and ERK MAP kinases *Oncogene* **25** 6563–73

Phys. Biol. 17 (2020) 036004, https://doi.org/10.1088/1478-3975/ab725c
Online movies: https://iopscience.iop.org/article/10.1088/1478-3975/ab725c/data

Supporting Information for "A biomechanical model for the extravasation of cancer cells"

S. M. Amin Arefi[1], Daria Tsvirkun[2,3], Claude Verdier[2] and James J. Feng[1,4*]

[1] Department of Chemical and Biological Engineering, University of British Columbia, Vancouver, BC V6T 1Z3, Canada
[2] University Grenoble Alpes, CNRS, LIPhy, 38000 Grenoble, France
[3] Belozersky Institute of Physico-chemical Biology, Lomonosov Moscow State University, Moscow 119991, Russia
[4] Department of Mathematics, University of British Columbia, Vancouver, BC V6T 1Z2, Canada

1 Mathematical model and numerics

For the extravasation of a tumor cell (TC) through the gap between endothelial cells (ECs), we set up a fluid-structure interaction problem, with partial differential equations describing the cytosol fluid flow and the elastic deformation of various elastic components—the TC membrane, the TC nucleus, the ECs and the extracellular matrix (ECM). Besides, the stress fiber (SF) and focal adhesion (FA) assembly evolves in time according to a set of differential and algebraic equations that describe the activation of actomyosin in the SF coupled with the growth of the FA. The main paper contains the equations governing SF and FA dynamics, cytosolic flow and elastic deformation of various components. In the following, we first list the complete set of governing equations, with additional supporting details regarding the FA mechanics. Then we describe the geometric setup and the boundary conditions for the wet-contact simulation. The dry-contact simulation is set up in a similar way, with the cytosolic flow and TC membrane omitted. We will end this section with a brief discussion of the numerical techniques used in the simulations.

(i) Complete set of governing equations. The SF dynamics is governed by a kinetic equation for

*Corresponding author. E-mail: james.feng@ubc.ca

actomyosin activation and a Hill-like constitutive equation for the SF:

$$\frac{d\eta}{dt} = (1-\eta)k_a e^{-\frac{t}{\theta}} - k_d\left(\eta - \frac{\tau}{\tau_{max}}\right), \tag{S1}$$

$$\tau = \begin{cases} 0, & \frac{v_f}{v_0} < -\frac{\eta}{k_v}, \\ \eta\tau_{max}\left(1 + \frac{k_v}{\eta}\frac{v_f}{v_0}\right), & -\frac{\eta}{k_v} \le \frac{v_f}{v_0} \le 0, \\ \eta\tau_{max}, & \frac{v_f}{v_0} > 0. \end{cases} \tag{S2}$$

Our FA model is based on the thermodynamic equilibrium between two conformational states of low- and high-affinity integrins, subject to the conservation of the total number of integrins: $\xi_H + \xi_L = \xi_0$. Only the high-affinity integrins contribute to the formation and growth of the FA; the tensile force τ in the SF is sustained by the FA and shared by all the high-affinity integrins in the FA:

$$k_B T \ln\frac{\xi_H}{\xi_L} = \Delta\mu - \Phi + F_b\, d_b, \tag{S3}$$

$$\tau = \xi_H F_b A_b, \tag{S4}$$

where k_B is the Boltzmann constant, T is temperature, and $\Delta\mu = \mu_L - \mu_H$ is the free energy difference between the low- and high-affinity integrins. The stretch energy Φ is expressed as a piecewise quadratic potential in the integrin bond length d_b, and the force $F_b = \partial\Phi/\partial d_b$ on each high-affinity integrin is piecewise linear:

$$\Phi = \begin{cases} \frac{1}{2}\lambda d_b^2, & d_b \le d_m, \\ -\lambda d_m^2 + 2\lambda d_m d_b - \frac{1}{2}\lambda d_b^2, & d_m < d_b \le 2d_m, \\ \lambda d_m^2, & d_b > 2d_m, \end{cases} \tag{S5}$$

$$F_b = \begin{cases} \lambda d_b, & d_b \le d_m, \\ 2\lambda d_m - \lambda d_b, & d_m < d_b \le 2d_m, \\ 0, & d_b > 2d_m. \end{cases} \tag{S6}$$

where λ is the stiffness of the bond and d_m is the maximum bond length.

The elastic components of the model, including the TC membrane, TC nucleus, the EC and the ECM, all obey the neo-Hookean constitutive equation, and the local force balance is expressed simply as the stress tensor having zero divergence:

$$\boldsymbol{\sigma} = G\, J^{-\frac{3}{5}}\left(\boldsymbol{F}\boldsymbol{F}^T - \frac{\boldsymbol{I}}{3}\operatorname{tr}\left(\boldsymbol{F}\boldsymbol{F}^T\right)\right) - K(J-1), \tag{S7}$$

$$\nabla\cdot\boldsymbol{\sigma} = 0. \tag{S8}$$

The elastic moduli differ among the various components and are listed in Section 2 below.

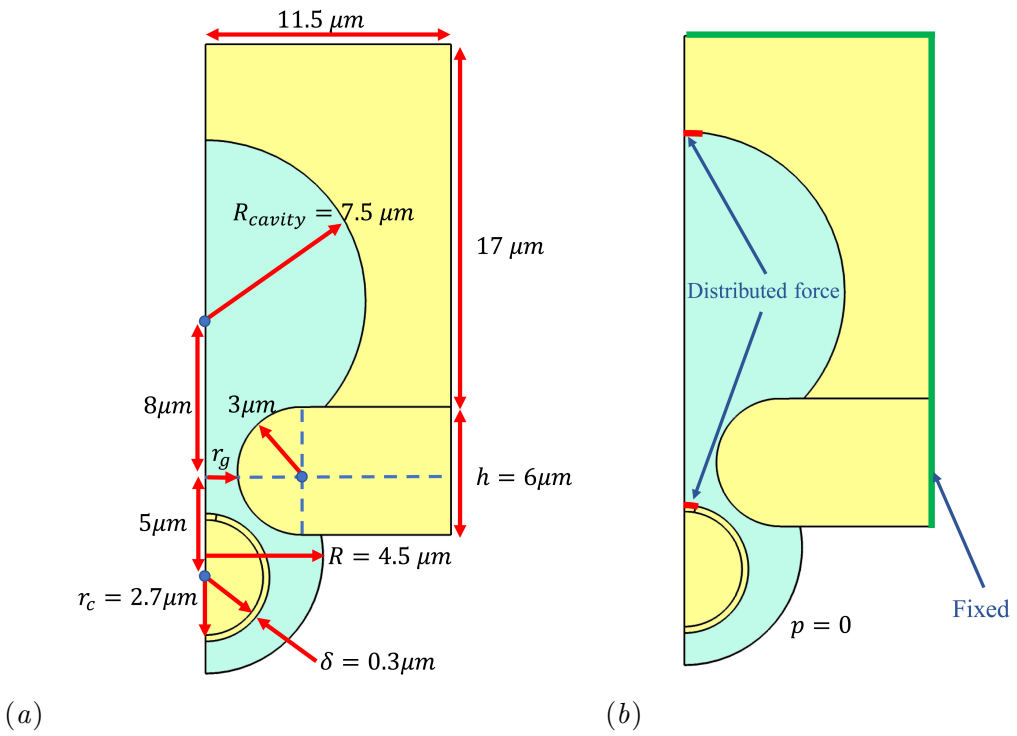

Figure S1: (a) The geometric setup for the so-called "wet-contact" simulation, with the cytosol and the membrane of the tumor cell explicitly represented. (b) Illustration of the boundary conditions. The green lines designate fixed boundaries and the red lines show boundaries with distributed forces.

The cytosolic flow is governed by the Navier-Stokes equations in the laminar flow regime:

$$\nabla \cdot \boldsymbol{v} = 0, \tag{S9}$$

$$\rho\left(\frac{\partial \boldsymbol{v}}{\partial t} + \boldsymbol{v} \cdot \nabla \boldsymbol{v}\right) = -\nabla p + \mu \nabla^2 \boldsymbol{v}. \tag{S10}$$

Finally, the displacement of the TC nucleus, the SF and FA stretching and the movement of the ECM at the FA are coupled by a kinematic condition, which completes the set of governing equations:

$$v_A + v_f + v_b = v_C. \tag{S11}$$

(ii) Geometric setup of the wet-contact simulation. The axisymmetric computational domain of the simulation is shown in Figure S1(a). The nucleus of the cancer cell is initially a sphere of radius $r_n = 3$ μm. It is made of a soft core of radius $r_c = 2.7$ μm and a stiffer shell of thickness $\delta = 0.3$ μm. The endothelium is represented by an elastic layer of thickness $h = 6$ μm. At the center of the endothelium is a circular hole of radius $r_g = 1.5$ μm; the rim of the hole is a circular arc of radius $h/2$. The ECM is treated as an elastic material with a cavity in the middle of initial radius of $R_{cavity} = 7.5$ μm. At the start, the TC nucleus is centered 5 μm below the centerline of the

EC and 13 μm below the center of the ECM cavity. The upper part of the TC membrane is not treated separately since it is in contact with the ECM. The lower part is a spherical shell that is initially concentric with the nucleus, with an inner radius of $R = 4.5$ μm and a thickness of $\epsilon = 10$ nm. The upper end of the TC membrane is attached onto the endothelium at the intersection of the round membrane and endothelial layer.

(iii) Boundary conditions. Around the outline of the computational domain, three types of boundary conditions are imposed. Along the axis of symmetry ($r = 0$), of course, all radial derivatives vanish. The outer boundaries of ECM and the endothelial layer, marked by the green lines in Fig. S1(b), are fixed in space with zero displacement. Finally, on the outside of the TC membrane we impose a constant ambient pressure $p = 0$.

On all the fluid-solid interfaces, including that between the cytosol and the ECM, the EC, the TC nucleus and the TC membrane, we impose continuity in the velocity $\boldsymbol{v}$ and traction:

$$\boldsymbol{v}_{solid} = \boldsymbol{v}_{fluid}, \tag{S12}$$

$$\boldsymbol{n} \cdot \boldsymbol{\sigma}_{solid} = \boldsymbol{n} \cdot \boldsymbol{\sigma}_{fluid}, \tag{S13}$$

$\boldsymbol{n}$ being the local unit normal vector. The tension inside the SF-FA assembly requires some special treatment. To avoid local singularities, we distribute the force τ in the stress fibers over a small area marked in red on top of the nucleus in Fig. S1(b), of area A_n. A uniform traction of magnitude τ/A_n is applied in the vertical direction over this area. Similarly, on the roof of the cavity where the FA meets the ECM, we distribute τ over the FA area A_b.

The dry-contact setup is similar and simpler, in that the TC cell membrane and cytosol are neglected. On solid surfaces exposed to the cytosol in the wet-contact setup, i.e. the inner surfaces of the ECM and the EC, as well as the TC nucleus, we now impose the zero-stress condition: $\boldsymbol{n} \cdot \boldsymbol{\sigma}_{solid} = 0$.

(iv) Numerical techniques. The numerical problem formulated in the above is solved by COMSOL Multiphysics, a finite-element package. The dry-contact simulation consists in solving for the elastic deformation of the various components under the driving force that develops inside the SF-FA complex. A prominent feature is the contact force between the nucleus and the EC. This is handled by the penalty method, a common technique in solving solid-contact problems [1].

The wet-contact simulations consist essentially in fluid-structure interactions, with coupled solutions of the cytosolic flow and the elastic deformation of the elastic components (ECM, EC and TC components). The cytosol in the thin gap between the TC nucleus and EC provides a lubricating pressure. In addition, we have found it necessary to introduce a repulsive pressure to prevent very close approach between the TC nucleus and the EC surface, which could cause numerical blowup. Such a repulsion is commonly used in the literature for preventing solid-solid contact across a narrow fluid gap [2]. This repulsive pressure is imposed on the nuclear and endothelial boundary nodes, and is defined using the shortest distance d from a node to the opposite surface:

$$P_{rep} = P_0 \, \frac{\tanh\left(d^{-1} - d_0^{-1}\right) + 1}{2}, \tag{S14}$$

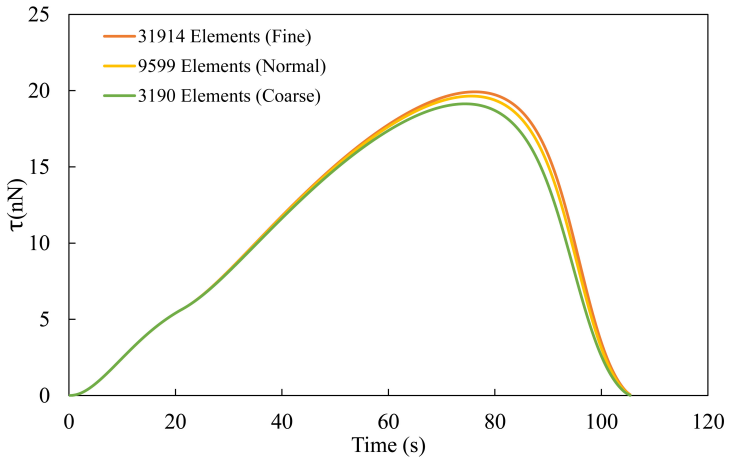

Figure S2: The effect of different mesh resolution on the contractile force in the stress fibers. The solutions using the coarse, normal and fine resolutions are sufficiently close, and we have used the normal resolution in all results reported later.

where $P_0 = 100$ kPa, $d_0 = 0.588$ μm and d is measured in micrometers. The value of d_0 determines how steeply P_{rep} decays with the separation d, and the minimum separation is about 0.25 μm during the transmigration under the standard set of parameters (see Section 2 below). We have tested P_0 values down to 50 and 10 kPa; the minimum gap size decreases to 0.24 μm and 0.15 μm, and the maximum tension in the stress fibers decreases from 70 nN to 65 nN and 57 nN, respectively. Therefore, in this range P_0 does not strongly affect the threshold for transmigration.

In our simulations, COMSOL does implicit time stepping, and adaptively refines or remeshes an unstructured triangular grid. We have done numerical experimentation to ensure adequate temporal and spatial resolutions. As an example, Fig. S2 shows the effect of mesh refinement on the contractile force in the stress fibers in the dry-contact simulation. All the results reported have used the so-called "normal resolution" with roughly 10,000 elements for the dry-contact setup, and 27,000 elements for the wet-contact setup, with the smallest and largest grid sizes being 0.007 μm and 1.98 μm, respectively. The maximum time step is $\Delta t = 0.05$ s, which is adequate for resolving the transients in the simulations.

2 Model parameters

The model parameters fall into 3 categories: geometric, physical and biochemical, and they are tabulated in Tables 1–3 in that order together with the sources for their values. Where possible, the parameters are evaluated by using experimental measurements from the literature or our own laboratory. Otherwise the values are chosen based on similar modeling and computational studies in the literature. In the following, we highlight several notable parameters.

Symbol	Description	Value	Sources
r_n	TC nuclear radius	3 µm	[3, 4]
δ	TC nuclear shell thickness	0.3 µm	[3]
ϵ	TC membrane thickness	10 nm	[5, 6]
r_m	initial TC membrane radius	4.5 µm	this work
R	initial ECM radius	7.5 µm	[3]
h	endothelial thickness	6 µm	[3, 7, 8]
r_g	endothelial gap radius	1.5 µm	[3, 4, 9]
A_b	focal adhesion area	4 µm^2	[10, 11]

Table 1: Geometric parameters used in our model. Additional lengths are marked and given in Fig. S1.

For the geometric dimensions listed in Table 1, we have largely modeled after the prior simulation of Cao *et al.* [3]. In particular, the EC thickness is taken to be $h = 6$ μm. Experimental literature reports smaller values of 3–4 μm [7]. Our larger value is an effective thickness for the endothelium that also includes the basement membrane outside the EC [8]. The initial TC membrane radius is chosen based on the typical size of a tumor cell.

Symbol	Description	Value	Sources
G_{EC}	EC shear modulus	1 kPa	[3, 12, 13]
G_{ECM}	ECM shear modulus	5 kPa	[14]
G_c	TC nuclear core shear modulus	5 kPa	[3, 15]
G_s	TC nuclear shell shear modulus	50 kPa	[3]
G_m	TC membrane shear modulus	2 MPa	[16]
ν	Poisson's ratio for all elastic components	0.3	[3]
μ	TC cytosol viscosity	10^{-3} Pa·s	[17]
ρ	TC cytosol density	1000 kg m^{-2}	[6]
κ	TC nuclear drag coefficient	0.1 kg/s	this work

Table 2: Physical parameters used in our model.

The physical parameters consist of the properties of the various elastic components and the cytosolic fluid (Table 2). To allow strain hardening in the elastic components at large strain, we adopt the neo-Hookean hyperelastic constitutive relationship for all the elastic components, i.e. the ECM, EC, TC nuclear shell and core and the TC membrane. The same Poisson ratio $\nu = 0.3$ is assumed for all these components, but their shear moduli differ, as given in Table 2. Note that the TC membrane is much more rigid than the ECM and EC; this is chosen based on reported elastic modulus for lipid bilayers [16]. The TC nucleus is the limiting factor in extravasation, and deserves a few more words here. Following Cao *et al.* [3], we consider the nucleus as made of a hyperelastic

shell that encases a softer core of chromatin and other structures, both layers being governed by neo-Hookean constitutive relationships. The shell consists mainly of a matrix of Lamin A/C, which affords it an higher stiffness than the inside of the nucleus. We have adopted a shear modulus of $G_s = 10G_c$ following Cao *et al.* [3]. Experiments showed that the viscosity and density of the cytosol are not significantly different from those of water [6, 17], and so we have chosen $\mu = 10^{-3}$ Pa·s and $\rho = 1000$ kg/m^3.

As explained in the main text, a "Darcy-like" drag $-\kappa \boldsymbol{v}$ is applied onto the TC nucleus. The coefficient κ is determined such that when the nucleus snaps through the constriction, it attains a realistic velocity. In an experiment on a fibroblast crawling through a constriction on a substrate, Davidson *et al.* [18] reported nuclear velocity of up to 2 μm/min. From the *in vitro* extravasation experimental of Chen *et al.* [9], we estimate an average velocity of 0.8 μm/min. The κ value used here gives an average velocity of 3.8 μm/min, on the same order of magnitude as the observations.

Symbol	**Description**	**Value**	**Sources**
θ	decay time for calcium signal	100 s	[19, 20]
k_a	myosin activation rate	0.1 s^{-1}	[19]
k_d	myosin deactivation rate	0.01 s^{-1}	[19]
τ_{max}	maximum tension in SF	100 nN	[10, 11, 21]
k_v	coefficient in SF constitutive equation	10	[19, 20]
v_0	reference shortening rate of SF	1 μm/s	[10, 22]
ξ_0	total number of integrins per unit area	5000 μm^{-2}	[19, 23]
$\Delta\mu$	free-energy difference between low/high-affinity integrins	$5k_BT$	[24]
λ	stiffness of integrin bond	0.15 nN/μm	[19]
d_m	maximum strain of integrin bond	130 nm	[19]

Table 3: Biochemical parameters used in our model. In evaluating $\Delta\mu$, we have taken $k_B = 1.381 \times 10^{-23}$ m^2 kg/(s^2 K) and $T = 310$ K.

Finally, the biochemical parameters of the model are tabulated in Table 3. Most of these are adopted from Deshpande *et al.* [19, 24]. The total number of high and low affinity integrins (ξ_0) in an isolated cell is taken to be 5000 μm^{-2} [19, 23].

3 Parametric studies

The "baseline" set of parameters tabulated in the previous section is used in all the simulation results presented in the main paper. Besides, we have also done some limited exploration of the parametric space, in particular to determine how the outcome of TC transmigration depends on key parameters, including the size of the gap (r_g) in the endothelium, the ECM rigidity and the time scale of the chemical signal that stimulates myosin activation. These explorations have been done in the dry-contact setup for its lower computational cost.

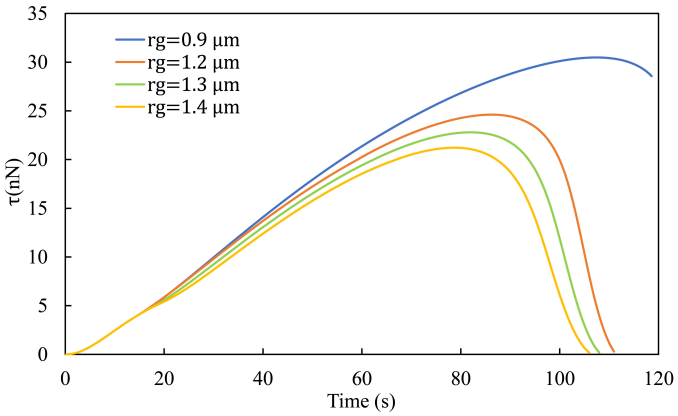

Figure S3: Effect of the EC gap radius r_g on extravasation of the TC nucleus in the dry-contact simulations. The outcome is depicted by the tension in the SF-FA assembly, and extravasation fails for too small a gap ($r_g \leq 0.9$ μm).

(i) Effect of the gap size. Figure S3 represents the impact of gap size on the driving force. As discussed in the main paper, a successful extravasation is characterized by a tension force τ that rises in time as the nucleus deforms and squeezes slowly through the gap, and falls precipitously upon breakthrough. Such is the case for the larger gaps ($r_g \geq 1.2$ μm). Note that as the gap shrinks in size, the force rises to larger values as the nucleus deforms more severely before transmigration occurs. It also takes longer time. For a gap that is too narrow ($r_g = 0.9$ μm), the nucleus becomes stuck and fails to extravasate, suggesting a critical ratio $r_g/r_n = 0.3 \sim 0.33$ for passage. Incidentally, the previous model of Cao *et al.* [3] predicts a critical ratio of $r_g/r_n = 0.3$ for the dry-contact setup, close to our predictions. This is also consistent with experimental observations that arrest happens at pores whose cross-sectional area is 10% of that of the nucleus [4].

(ii) Effect of ECM rigidity. Figure S4(a) shows the effect of shear modulus G_{ECM} of the ECM on the driving force τ due to SF contractility. The key observation is that a stiffer ECM facilitates transmigration. For $G_{ECM} \geq 500$ Pa, the ECM is sufficiently stiff to provide secure anchoring for the SF-FA machinery such that the latter produces a sharply rising τ to pull the nucleus through. Increasing ECM modulus makes the passage faster. On the other hand, softening the ECM below 500 Pa has a more qualitative effect and transmigration eventually fails for $G_{ECM} \leq 100$ Pa. As illustrated by the snapshot in Fig. S4(b), the soft ECM deforms greatly in response to the tension in the stress fibers, and the nucleus remains stuck at the endothelial gap. This again illustrates the importance of having a secure anchoring pad for the contractile machinery.

The effect the ECM rigidity can be compared with the effect of the cantilever speed in measuring the extravasation force (Fig. 11 of the main text). A higher cantilever speed leaves the ECs less time to relax and adapt to the deformation brought on by the TC, and thus the ECs will appear more rigid. As a result, the force rises more rapidly in Fig. 11, similar to the trend in Fig. S4(a). Conversely, a slower cantilever speed leads to effectively softer ECs and a slower increase in the force. The two situations differ, however, in that softer ECs favor extravasation in the experiment while a softer ECM impedes extravasation here.

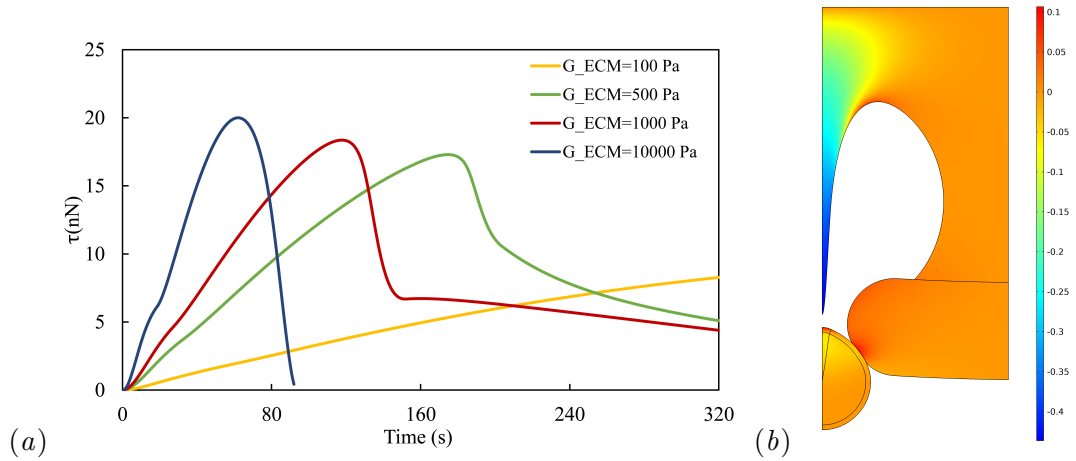

Figure S4: Effect of the ECM modulus G_{ECM} on extravasation of the TC nucleus in the dry-contact simulations. (a) Temporal evolution of the tension τ for 4 values of the ECM modulus. Extravasation fails if the ECM is too soft ($G_{ECM} \leq 100$ Pa). (b) A snapshot of the ECM deformation at $t = 210$ s for $G_{ECM} = 100$ Pa shows great deformation of the soft ECM that accompanies failure of extravasation. The color contours indicate the vertical component of the stretching.

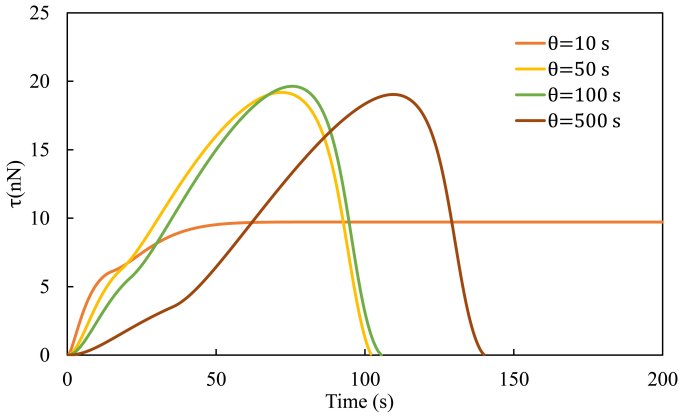

Figure S5: Effect of time scale θ of the activation signal (see Eq. S1). Transmigration requires a minimum θ, which is between 10 and 50 s.

(iii) Effects of duration of the activating signal. In our biochemical model, the actomyosin activation is driven by a chemical signal, e.g. an ionic influx of Ca^{2+}. In Eq. (S1), this signal decays exponentially in time with a time constant θ. Figure S5 plots the time evolution of the contractile force τ for four values of θ. If we lengthen θ from the baseline value of $\theta = 100$ s, the contractile force τ grows more slowly initially, but in time reaches a similar maximum before declining. The passage takes a longer time to complete. As we shorten θ, however, the decay of the stimulating signal is faster, and τ achieves a relatively low maximum force. For $\theta \leq 10$ s, this maximum falls below what is needed to deform the nucleus sufficiently and transmigration fails.

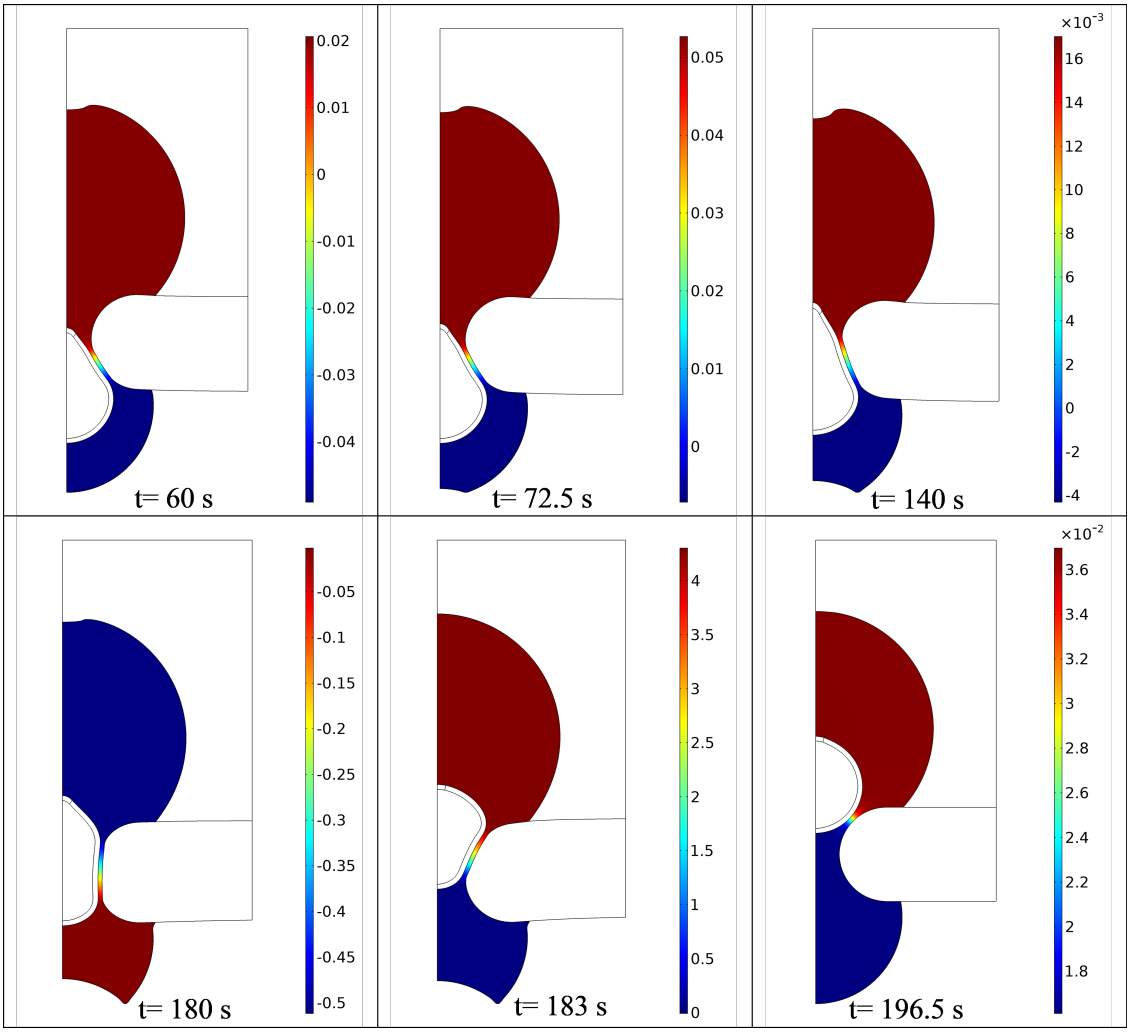

Figure S6: Evolution of the pressure field in the cytosol during various stages of the extravasation.

4 Effect of cytosolic flow

As the tumor-cell nucleus transmigrates in the cytosol, one expects its movement to raise the pressure upstream of the nucleus and reduce the pressure downstream. This in turn may incur a downward cytosolic flow in the lubricating film separating the nucleus from the membrane. Both effects should hinder the nucleus motion. Besides, Cao *et al.* [3] discussed how the static Laplacian pressure may produce a net force for or against transmigration by assuming a uniform and constant membrane tension. In our model, we assume no preexisting cortical tension in the TC membrane; it is initially in an undeformed state with zero tension. Besides, the initial pressure in the cytosol is zero. The ambient pressure in the "blood vessel", i.e. below the endothelium, is maintained at zero for all times. Thus, we ignore the Laplacian pressure and focus on the hydrodynamic effects of the cytosolic flow.

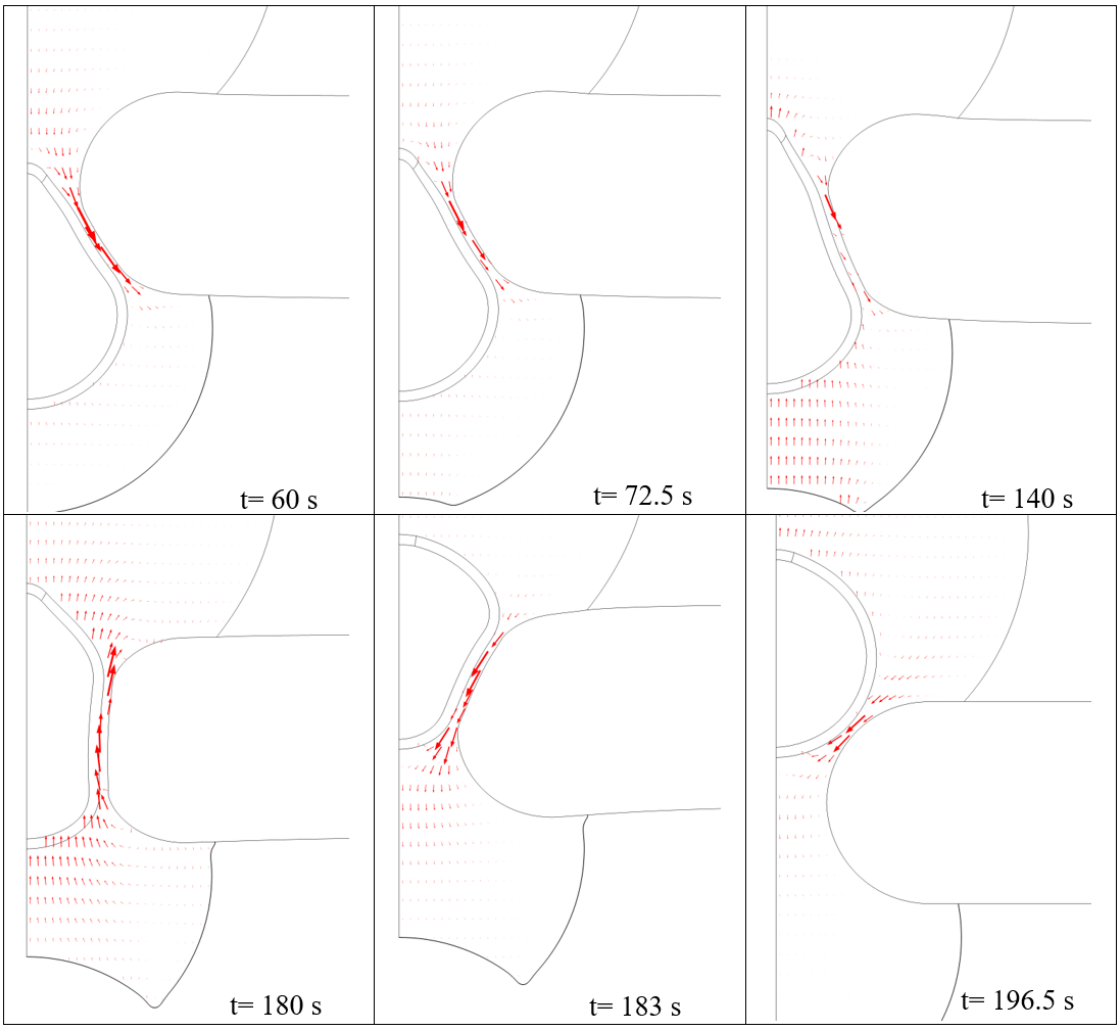

Figure S7: Velocity field in the cytosol during various stages of the extravasation.

Our dynamic simulation shows interesting temporal changes in the pressure and flow field in the cytosol during the transmigration. Figures S6 and S7 show snapshots of the pressure distribution and velocity vectors during the passage of the nucleus. When the nucleus approaches the constriction ($t = 60$ s), it behaves like a piston and raises the pressure in the upper chamber relative to the lower chamber. This pressure field pumps the cytosol downward through the thin gap between the nucleus and the EC. At $t = 72.5$ s, the pressure at the lower chamber becomes so low that the membrane caves in. The same overall pattern of pressure distribution and downward cytosolic flow prevails for the entire process of extravasation except for a short interval around $t = 180$ in which the pressure gradient becomes inverted, with lower pressure upstream of the nucleus and the upward flow in the thin gap.

The cause of the anomalous pressure gradient at $t = 180$ s is not entirely clear, but appears to be related to the rapid acceleration of the nucleus once it breaks through the point of greatest constriction (cf. Fig. 8 in the main text). We speculate that it may have arisen from the compress-

ibility of the elastic components coupled with the large difference in rigidity between the ECM and the TC membrane. Since the ECM is much softer than the TC membrane (Table 2), it deforms more readily as the nucleus pushes into the upper cavity and causes it to expand. For a short period, the expansion of the upper chamber may be such that the pressure becomes lower. The inertia of the cytosolic flow may also become appreciable during the nuclear acceleration, but it is unclear whether it plays a role in the pressure inversion. Because of the short duration of the inverted pressure, it has little impact on the nuclear transmigration.

Overall, the hydrodynamic pressure and the cytosolic flow both act to resist the transmigration. But their magnitudes are much smaller than the dominant forces of the process—the contractile force in the stress fibers and the elastic resistance of the endothelium. For example, the maximum pressure force on the nucleus, achieved at $t \approx 183$ s, is about 55 pN, while the maximum viscous shear force is only 6 pN. Therefore, the cytosol affects the nuclear transmigration mostly through the lubricating layer. The direct contribution of the back pressure and viscous friction is negligible.

5 Supplemental Movies

Two supplemental movies can be downloaded from the article's home page. Below are their captions.

Movie 1: Animation of the dry-contact simulation of transmigration of a tumor-cell nucleus. The color contours indicate the vertical component of the elastic strain.

Movie 2: Animation of the wet-contact simulation of transmigration of a tumor cell. The color contours inside the solids (corresponding to the left color bar) indicate the vertical component of the elastic strain, while those in the cytosol (right color bar) indicate the magnitude of the velocity in m/s.

References

[1] P. Wriggers, Computational Contact Mechanics, Springer-Verlag Berlin Heidelberg, 2006.

[2] T. Wu, J. J. Feng, Modeling the mechanosensitivity of neutrophils passing through a narrow channel, Biophys. J. 109 (11) (2015) 2235–2245.

[3] X. Cao, E. Moeendarbary, P. Isermann, P. Davidson, X. Wang, M. Chen, A. Burkart, J. Lammerding, R. Kamm, V. Shenoy, A chemomechanical model for nuclear morphology and stresses during cell transendothelial migration, Biophys. J. 111 (7) (2016) 1541 – 1552.

[4] K. Wolf, M. Te Lindert, M. Krause, S. Alexander, J. Te Riet, A. L. Willis, R. M. Hoffman, C. G. Figdor, S. J. Weiss, P. Friedl, Physical limits of cell migration: control by ECM space and nuclear deformation and tuning by proteolysis and traction force, J. Cell Biol. 201 (7) (2013) 1069–1084.

[5] J. Escribano, M. B. Chen, E. Moeendarbary, X. Cao, V. Shenoy, J. M. Garcia-Aznar, R. D. Kamm, F. Spill, Balance of mechanical forces drives endothelial gap formation and may facilitate cancer and immune-cell extravasation, PLoS Comput. Biol. 15 (5) (2019) e1006395.

[6] U. Moran, R. Phillips, R. Milo, Snapshot: key numbers in biology, Cell 141 (7) (2010) 1262–1262.

[7] M. Sato, K. Nagayama, N. Kataoka, M. Sasaki, K. Hane, Local mechanical properties measured by atomic force microscopy for cultured bovine endothelial cells exposed to shear stress, J. Biomech. 33 (1) (2000) 127–135.

[8] A. L. James, P. S. Maxwell, G. Pearce-Pinto, J. G. Elliot, N. G. Carroll, The relationship of reticular basement membrane thickness to airway wall remodeling in asthma, Am. J. Respir. Crit. Care Med. 166 (12) (2002) 1590–1595.

[9] M. B. Chen, J. A. Whisler, J. S. Jeon, R. D. Kamm, Mechanisms of tumor cell extravasation in an in vitro microvascular network platform, Integr. Biol. 5 (10) (2013) 1262–1271.

[10] A. Besser, U. S. Schwarz, Coupling biochemistry and mechanics in cell adhesion: a model for inhomogeneous stress fiber contraction, New J. Phys. 9 (2007) 425.

[11] J. L. Tan, J. Tien, D. M. Pirone, D. S. Gray, K. Bhadriraju, C. S. Chen, Cells lying on a bed of microneedles: an approach to isolate mechanical force, Proc. Natl. Acad. Sci. U.S.A. 100 (4) (2003) 1484–1489.

[12] H. Sato, N. Kataoka, F. Kajiya, M. Katano, T. Takigawa, T. Masuda, Kinetic study on the elastic change of vascular endothelial cells on collagen matrices by atomic force microscopy, Colloids Surf. B 34 (2) (2004) 141–146.

[13] A. B. Mathur, A. M. Collinsworth, W. M. Reichert, W. E. Kraus, G. A. Truskey, Endothelial, cardiac muscle and skeletal muscle exhibit different viscous and elastic properties as determined by atomic force microscopy, J. Biomech. 34 (12) (2001) 1545–1553.

[14] M. J. Paszek, N. Zahir, K. R. Johnson, J. N. Lakins, G. I. Rozenberg, A. Gefen, C. A. Reinhart-King, S. S. Margulies, M. Dembo, D. Boettiger, et al., Tensional homeostasis and the malignant phenotype, Cancer Cell 8 (3) (2005) 241–254.

[15] N. Caille, O. Thoumine, Y. Tardy, J.-J. Meister, Contribution of the nucleus to the mechanical properties of endothelial cells, J. Biomech. 35 (2) (2002) 177–187.

[16] A. Vaziri, M. R. K. Mofrad, Mechanics and deformation of the nucleus in micropipette aspiration experiment, J. Biomech. 40 (9) (2007) 2053–2062.

[17] S. Bicknese, N. Periasamy, S. Shohet, A. Verkman, Cytoplasmic viscosity near the cell plasma membrane: measurement by evanescent field frequency-domain microfluorimetry, Biophys. J. 65 (3) (1993) 1272–1282.

[18] P. M. Davidson, J. Sliz, P. Isermann, C. Denais, J. Lammerding, Design of a microfluidic device to quantify dynamic intra-nuclear deformation during cell migration through confining environments, Integr. Biol. 7 (12) (2015) 1534 – 1546.

[19] V. S. Deshpande, R. M. McMeeking, A. G. Evans, A model for the contractility of the cytoskeleton including the effects of stress-fibre formation and dissociation, Proc. R. Soc. London, Ser. A 463 (2079) (2007) 787–815.

[20] W. Ronan, V. S. Deshpande, R. M. McMeeking, J. P. McGarry, Cellular contractility and substrate elasticity: a numerical investigation of the actin cytoskeleton and cell adhesion, Biomech. Model. Mechanobiol. 13 (2) (2014) 417–435.

[21] N. Q. Balaban, U. S. Schwarz, D. Riveline, P. Goichberg, G. Tzur, I. Sabanay, D. Mahalu, S. Safran, A. Bershadsky, L. Addadi, et al., Force and focal adhesion assembly: a close relationship studied using elastic micropatterned substrates, Nat. Cell Biol. 3 (5) (2001) 466.

[22] K. Katoh, Y. Kano, M. Masuda, H. Onishi, K. Fujiwara, Isolation and contraction of the stress fiber, Mol. Biol. Cell 9 (7) (1998) 1919–1938.

[23] D. A. Lauffenburger, J. J. Linderman, Receptors: models for binding, trafficking, and signaling, Oxford University Press, 1996.

[24] V. S. Deshpande, M. Mrksich, R. M. McMeeking, A. G. Evans, A bio-mechanical model for coupling cell contractility with focal adhesion formation, J. Mech. Phys. Solids 56 (4) (2008) 1484 – 1510.